KN and $\bar{K}N$ elastic scattering in the quark potential model

Hai-Jun Wang,[1] Hui Yang,[1] and Jun-Chen Su[1,2,*]
[1]*Center for Theoretical Physics, College of Physics, Jilin University, Changchun 130023, People's Republic of China*
[2]*Department of Physics, Harbin Institute of Technology, Harbin 150006, People's Republic of China*
(Received 2 April 2003; revised manuscript received 4 August 2003; published 26 November 2003)

The KN and $\bar{K}N$ low-energy elastic scattering is consistently studied in the framework of the QCD-inspired quark potential model. The model is composed of the t-channel one-gluon exchange potential, the s-channel one-gluon exchange potential, and the harmonic oscillator confinement potential. By means of the resonating group method, nonlocal effective interaction potentials for the KN and $\bar{K}N$ systems are derived and used to calculate the KN and $\bar{K}N$ elastic scattering phase shifts. By considering the effect of QCD renormalization, the contribution of the color octet of the clusters $(q\bar{q})$ and (qqq), and the suppression of the spin-orbital coupling, the numerical results are in fairly good agreement with the experimental data.

DOI: 10.1103/PhysRevC.68.055204 PACS number(s): 13.75.Jz, 12.39.−x, 14.20.Jn, 25.80.Nv

I. INTRODUCTION

Inspired by the achievement in the study of hadron spectroscopy within the framework of quark potential model [1–3], there have been continuous efforts to apply the quark potential model and the resonating group method (RGM) [4] to study nucleon-nucleon, nucleon-meson, and meson-meson interactions and scattering [5–20]. Among these efforts, the study of kaon-nucleon (KN) interaction arose a particular interest in the past. Due to the high penetrating power of K^+ meson, it is expected that the study of K^+N interaction would provide more information for nuclear structures and properties. Since in the K^+N interaction, the one-pion exchange is forbidden, the two-pion exchange is suppressed [10,11] and there is no annihilation of valence quarks to appear, it is expected that the t-channel one-gluon exchange potential (OGEP) plus the harmonic oscillator confinement potential would give a reasonable description of the K^+N interaction. With this idea, the authors in Ref. [10] calculated the S-wave phase shifts of K^+N elastic scattering and found that the theoretical results are in quite good agreement with the experimental data in the low-energy domain. It is noted that in the calculation, the authors only took the Coulomb, spin-spin, and Darwin terms in the t-channel OGEP without considering the spin-orbital coupling and tensor force terms which contribute to the higher partial wave scattering. Subsequently, to investigate P-wave phase shifts, the authors in Ref. [11] introduced into their model the spin-orbital coupling terms originating from the t-channel one-gluon exchange and a scalar exchange term describing the confinement interaction. As one knows, there are two kinds of spin-orbit coupling terms in the t-channel OGEP: the spin-symmetric term and the spin-antisymmetric one. Correspondingly, there also exist two such terms in the confining potential generated from the scalar exchange. The spin-symmetric terms in the two potentials have opposite signs. Therefore, the effect of the spin-orbital coupling is suppressed just as required in the study of meson and baryon spectra [2,21]. However, the spin-antisymmetric terms are of the same sign and hence would produce large splitting, which is in contradiction with the experiment [11]. Such terms are therefore dropped out in Ref. [11]. The calculation in Ref. [11] showed that if the spin-orbit coupling terms are considered only, except for the $I=0$, $J=\frac{1}{2}$ channel phase shift, the sign and magnitude of the other channel phase shifts are well reproduced; when the other terms in the t-channel OGEP are taken into account together, there appears a serious problem that the $I=1$ channel phase shifts all become negative, conflicting with the experimental data. Later, the S-wave phase shifts of KN scattering are restudied in Ref. [15] by employing the Born order diagrammatic technique. In the study, although only the spin-spin coupling term in the t-channel OGEP is considered, the calculated result looks fine. Subsequently, the Born approximation was applied to investigate the KN scattering more extensively in Ref. [17]. In the investigation, apart from the hyperfine term in the OGEP and the linear scalar confinement, the spin-orbital coupling and spin-independent terms in the OGEP are taken into account in the evaluation of P-wave and D-wave phase shifts. Nevertheless, the magnitudes of most of the calculated phase shifts are smaller than the experimental ones. Particularly, the sign of the theoretical P_{13} wave phase shift is opposite to the experimental data. Recently, the KN phase shifts are recalculated in Ref. [18] within the constituent quark model by numerically solving the Hill-Wheeler equation, trying to give a consistent description for the KN interaction and the relevant meson and baryon spectra. In the calculation, besides the linear confining potential, the authors used only the Coulomb term and the spin-spin interaction term multiplied by a phenomenological coefficient function of Gaussian type. The calculated $I=0$ channel S-wave phase shift is quite good in comparison with the experiment; whereas for the $I=1$ channel S-wave phase shift, there appears a big discrepancy between the theoretical result and the experimental one. The authors also calculated higher angular momentum phase shifts without including the spin-orbit coupling and tensor force terms in the OGEP. Even though the results were considered to be quite reasonable, the calcula-

*Corresponding author. Email address: junchens@public.cc.jl.cn

tion is not complete theoretically because the spin-orbit coupling and tensor force terms in the OGEP were not taken into account.

From the previous works mentioned above, it is clearly seen that a precise understanding of the KN interaction at quark-gluon level still calls for a sophisticated quark potential model which can give a consistently good description for not only the KN interaction, but also the $\bar{K}N$ interaction which has never been investigated in the past. For this purpose, it is necessary to incorporate new physical ingredients into the model as suggested in Refs. [11,18]. In this paper, we attempt to investigate the KN and $\bar{K}N$ interactions and their low-energy elastic phase shifts in a consistent way within the quark potential model. The new features of this investigation include the following.

(1) The potential model is composed of the t-channel OGEP [1] and the s-channel OGEP [22] as well as a phenomenological confining potential. The t-channel OGEP is responsible for the KN interaction, while for the $\bar{K}N$ interaction where the annihilation and creation of a quark-antiquark ($q\bar{q}$) pair appear, the s-channel OGEP is necessary to be considered as demonstrated in our previous investigations of $\pi\pi$ and $K\bar{K}$ interactions [19,20]. In these investigations, it was shown that the s-channel OGEP plays a dominant role for the $\pi\pi$ $I=0$ channel S-wave scattering and is necessary to be considered for the formation of $K\bar{K}$ molecular states. As one knows, the two OGEPs are derived from QCD in the nonrelativistic approximation of order p^2/m^2 and contain spin-independent terms (such as the Coulomb), velocity-dependent terms, and spin-dependent terms (such as the spin-spin interaction, spin-orbital coupling, and tensor force terms). All these terms are taken into account in our calculation as should be done in a theoretically consistent treatment.

(2) Inclusion of the QCD renormalization effect. It is well known that the OGEPs are derived from the tree diagram approximation of the S-matrix elements or the irreducible interaction kernels in the Bethe-Salpeter (BS) equation. Obviously, to refine the potential model, the QCD renormalization effect is necessary to be incorporated into the model. This can be done by replacing the QCD coupling constant and quark masses in the OGEP with their effective ones which were derived in our previous work in the one-loop approximation and a mass-dependent momentum space subtraction [23]. Our calculation indicates that the inclusion of the QCD renormalization effect gives an appreciable improvement on the theoretical phase shifts, particularly, for the P-wave phase shifts.

(3) The contribution from the color octet of the three-quark cluster (qqq) and the quark-antiquark cluster $(q\bar{q})$ to the KN and $\bar{K}N$ scattering is considered because when the kaon (antikaon) and nucleon interact, the color singlet states of the clusters (qqq) and $(q\bar{q})$ are possibly polarized. This consideration has been justified in the recent studies of meson production and decay phenomena [24,25]. In these studies, the color octet of $q\bar{q}$ cluster plays an essential role in explaining the experimental data. According to our calculation, the consideration of color octet can also improve the theoretical results.

(4) Nonlocal KN and $\bar{K}N$ effective interaction potentials are derived from the underlying interquark potentials by employing the RGM and used to evaluate the phase shifts. We do not use the localized version of the potentials because an inappropriate localization would damage the Hermiticity of the potentials and induce other unexpected errors.

(5) The effect of spin-orbital coupling in the t-channel OGEP is necessarily suppressed in the present investigation in order to reproduce the P-wave phase shifts. This is consistent with the requirement in the study of hadron spectroscopy. The suppression may be achieved by a proper change of the coefficient function of the spin-orbit term in the effective intercluster potentials which are derived from the corresponding term in the OGEP. With the considerations mentioned above, we obtain in this paper a series of theoretical KN S-wave, P-wave, and D-wave phase shifts which are in fairly good agreement with the experimental data. In addition, a series of theoretical phase shifts for the $\bar{K}N$ elastic scattering are predicted.

The rest of this paper is arranged as follows: Section II is used to describe the quark potential model and show how to derive the KN and $\bar{K}N$ effective interaction potentials. Section III serves to describe the calculation of the KN and $\bar{K}N$ scattering phase shifts. In the last section, the calculated results are presented and discussions are made. There are four appendixes. In Appendix A, we show the construction of the color-flavor-spin wave function for the systems under consideration. In Appendix B, the effective KN and $\bar{K}N$ interaction potentials derived in position space are listed. In Appendix C, we briefly describe the derivation of the phase-shift formula used in our calculation. Appendix D is used to make some explanations on the QCD renormalization.

II. QUARK POTENTIAL MODEL AND EFFECTIVE KN AND $\bar{K}N$ POTENTIALS

According to the quark model, the KN ($\bar{K}N$) system may be treated as two-quark clusters: the K-cluster $(q\bar{s})$ [the $\bar{K}$-cluster $(\bar{q}s)$] and the N cluster (qqq), where $q=u$ or d. The effective KN interaction potential may be extracted from the following Schrödinger equation for the interacting $q^4\bar{s}$ system by the RGM:

$$(T+V)\Psi = E\Psi, \tag{1}$$

where E, T, V, and Ψ stand for the total energy, the kinetic energy, the interaction potential, and the wave function of the system, respectively. In the center of mass frame,

$$T = \sum_i \frac{\vec{p}_i^{\,2}}{2m_i} - T_c, \tag{2}$$

where T_c represents the center of mass kinetic energy,

$$V = \sum_{i<j=1}^{5} (V_{ij}^t + V_{ij}^s + V_{ij}^c), \tag{3}$$

here V_{ij}^t, V_{ij}^s, and V_{ij}^c denote the t-channel OGEP, the s-channel OGEP, and the confining potentials, respec-

tively. They are separately written in the following. The *t*-channel OGEP represented in the momentum space [26] is

$$V_{ij}^{t}=\frac{4\pi\alpha_s C_{ij}^{t}}{(\vec{q}-\vec{k})^2}\Bigg\{1-\frac{\vec{P}^2}{m_{ij}^2}-\frac{(m_i^2+m_j^2)}{8m_i^2m_j^2}(\vec{q}-\vec{k})^2+\frac{(m_i-m_j)}{2m_im_jm_{ij}}\vec{P}\cdot(\vec{q}+\vec{k})+\frac{(\vec{q}+\vec{k})^2}{4m_im_j}+\frac{i}{4m_{ij}}\left[\vec{P}\cdot(\vec{q}-\vec{k})\cdot\left(\frac{\vec{\sigma}_i}{mi}-\frac{\vec{\sigma}_j}{m_j}\right)\right]-\frac{(\vec{q}-\vec{k})^2}{4m_im_j}\vec{\sigma}_i\cdot\vec{\sigma}_j+\frac{i}{4m_{ij}}(\vec{q}\times\vec{k})\cdot\left[\left(2+\frac{m_j}{m_i}\right)\vec{\sigma}_i+\left(2+\frac{m_i}{m_j}\right)\vec{\sigma}_j\right]+\frac{(\vec{q}-\vec{k})\cdot\vec{\sigma}_i(\vec{q}-\vec{k})\cdot\vec{\sigma}_j}{4m_im_j}\Bigg\} \tag{4}$$

where $m_{ij}=m_i+m_j$, α_s is the QCD fine structure constant, $\vec{\sigma}_i$ are the spin Pauli matrices for *i*th particle, and C_{ij}^{t} is the *t*-channel color matrix defined as

$$C_{ij}^{t}=\begin{cases}\dfrac{\lambda_i^a}{2}\dfrac{\lambda_j^a}{2}\left(\dfrac{\lambda_i^{a*}}{2}\dfrac{\lambda_j^{a*}}{2}\right) & \text{for } qq(\overline{qq})\\ -\dfrac{\lambda_i^a}{2}\dfrac{\lambda_j^{a^*}}{2} & \text{for } q\bar{q},\end{cases} \tag{5}$$

with λ^a being the Gell-Mann matrix, $\vec{P},\vec{k}$, and $\vec{q}$ are the total momentum, the initial state relative momentum, and the final state relative momentum of the two interacting particles.

The *s*-channel OGEP [20,22] is

$$V_{ij}^{s}=\frac{\pi\alpha_s F_{ij}^{s}C_{ij}^{s}}{2mm'}\Bigg[(3+\vec{\sigma}_i\cdot\vec{\sigma}_j)-\frac{5(m^2+m'^2)-4m'}{8m^2m'^2}\vec{P}^2-\frac{2\vec{k}^2}{m^2}-\frac{2\vec{q}^2}{m'^2}-\left(\frac{(m^2+m'^2)}{8m^2m'^2}+\frac{\vec{k}^2}{m^2}+\frac{\vec{q}^2}{m'^2}\right)\vec{\sigma}_i\cdot\vec{\sigma}_j+\frac{i}{4m'^2}(\vec{P}\times\vec{q})\cdot(\vec{\sigma}_i-\vec{\sigma}_j)-\frac{i}{4m^2}(\vec{P}\times\vec{k})\cdot(\vec{\sigma}_i-\vec{\sigma}_j)-\frac{(m-m')^2}{4m^2}\vec{P}\cdot\vec{\sigma}_i\vec{P}\cdot\vec{\sigma}_j+\frac{1}{4m^2}(\vec{P}\cdot\vec{\sigma}_i\vec{k}\cdot\vec{\sigma}_j-\vec{k}\cdot\vec{\sigma}_i\vec{P}\cdot\vec{\sigma}_j+4\,\vec{k}\cdot\vec{\sigma}\vec{k}\cdot\vec{\sigma}_j)+\frac{1}{4m'^2}(\vec{P}\cdot\vec{\sigma}_i\vec{q}\cdot\vec{\sigma}_j-\vec{q}\cdot\vec{\sigma}_i\vec{P}\cdot\vec{\sigma}_j+4\vec{q}\cdot\vec{\sigma}_i\vec{q}\cdot\vec{\sigma}_j)\Bigg], \tag{6}$$

where m and m' denote the quark (antiquark) masses before and after annihilation, respectively, C_{ij}^{s} and F_{ij}^{s} are the *s*-channel color and flavor matrices, defined by

$$C_{ij}^{s}=\frac{1}{24}(\lambda_i^a-\lambda_j^{a*})^2 \tag{7}$$

and

$$F_{ij}^{s}=\frac{2}{3}-\left(\frac{1}{2}\vec{\tau}_i\cdot\vec{\tau}_j+V_i^{-}V_j^{+}+V_i^{+}V_j^{-}+U_i^{-}U_j^{+}+U_i^{+}U_j^{-}+\frac{3}{2}Y_iY_j\right), \tag{8}$$

here $\vec{\tau}_i$ are the isospin Pauli matrices for the *i*th particle, Y_i the hypercharge operators, V_i^{+} and V_i^{-}(U_i^{+} and U_i^{-}) represent the rising and lowering operators of the *V* spin (*U* spin).

The confining potential, as was done in Refs. [10,11], is taken to be the harmonic oscillator one. In the momentum space it is represented as

$$V_{ij}^{c}=C_{ij}^{t}(2\pi)^3\mu_{ij}\omega^2\nabla_k^2\delta^3(\vec{q}-\vec{k}), \tag{9}$$

where μ_{ij} is the reduced mass of the interaction particles and ω force-strength parameter.

Now let us construct the wave function of the *KN* system from the wave functions of clusters $(q\bar{s})$ and (qqq). Since there are identical particles between the two clusters, the basis function of the system may be represented as

$$\Phi_{TMsm}(\vec{p}_1,\vec{p}_2,\vec{p}_3,\vec{p}_4,\vec{p}_5;\vec{\rho})=\frac{1}{\sqrt{4}}(1-P_{14}-P_{24}-P_{34})\Psi_{TM(1/2)m}(1,2,3,4,5)\times R(\vec{p}_1,\vec{p}_2,\vec{p}_3,\vec{p}_4,\vec{p}_5;\vec{\rho}) \tag{10}$$

where we number the three quarks in the *N* cluster as 1,2,3, and the quark and antiquark in the *K* cluster (or the antiquark and quark in the $\bar{K}$ cluster) as 4 and 5, $P_{j4}(j=1,2,3)$ symbolize the interchange operators, $\Psi_{TM(1/2)m}(1,2,3,4,5)$ and $R(\vec{p}_1,\vec{p}_2,\vec{p}_3,\vec{p}_4,\vec{p}_5;\vec{\rho})$ represent the color-isospin-spin wave function and the position space wave function respectively which are constructed from the color-isospin-spin wave functions and the coordinate space wave functions of nucleon and kaon. For the $\bar{K}N$ system, noticing that there is no identical particles between the two clusters $(\bar{q}s)$ and (qqq), the basis wave function of the system may simply be written as

$$\Phi_{TMsm}(\vec{p}_1,\vec{p}_2,\vec{p}_3,\vec{p}_4,\vec{p}_5;\vec{\rho})=\Psi_{TM(1/2)m}(1,2,3,4,5)R(\vec{p}_1,\vec{p}_2,\vec{p}_3,\vec{p}_4,\vec{p}_5;\vec{\rho}), \tag{11}$$

where $\Psi_{TM(1/2)m}(1,2,3,4,5)$ and $R(\vec{p}_1,\vec{p}_2,\vec{p}_3,\vec{p}_4,\vec{p}_5;\vec{\rho})$ are the color-isospin-spin wave function and the position space wave function constructed from the corresponding wave functions of nucleon and antikaon.

Since the *KN* system is treated as two clusters, when they interact, each cluster may be in color singlet $\underline{1}$ or in color octet $\underline{8}$ as indicated in Refs. [12,20]. Thus, the color-spin-isospin wave function $\Psi_{TM(1/2)m}(1,2,3,4,5)$ of the whole system may be given by the color singlet part $\Psi^{(1)}_{TM(1/2)m}\times(1,2,3,4,5)$ or the color octet part $\Psi^{(2)}_{TM(1/2)m}(1,2,3,4,5)$ formed by the color singlets or color octets of the two clusters. In principle, we may test a general color structure of system under consideration which is given by the following linear combination:

$$\Psi_{TM(1/2)m}(1,2,3,4,5) = \alpha\Psi^{(1)}_{TM(1/2)m}(1,2,3,4,5) + \beta\Psi^{(2)}_{TM(1/2)m}(1,2,3,4,5), \tag{12}$$

where the coefficients α and β are required to satisfy

$$|\alpha|^2 + |\beta|^2 = 1. \tag{13}$$

The wave functions $\Psi^{(1)}_{TM(1/2)m}(1,2,3,4,5)$ and $\Psi^{(2)}_{TM(1/2)m}\times(1,2,3,4,5)$ are listed in Appendix A. They are constructed by antisymmetry of the wave functions of identical particles in nucleon.

Because we limit our discussion to the interaction in the low-energy regime, it is appropriate to write the position space basis function of the KN or $\overline{K}N$ system in the form

$$R(\vec{p}_1,\vec{p}_2,\vec{p}_3,\vec{p}_4,\vec{p}_5;\vec{\rho}) = \phi^{(+)}_{os}(\vec{p}_1,\vec{\rho})\phi^{(+)}_{os}(\vec{p}_2,\vec{\rho})\phi^{(+)}_{os}(\vec{p}_3,\vec{\rho})\phi^{(-)}_{os}\times(\vec{p}_4,\vec{\rho})\phi^{(-)}_{os}(\vec{p}_5,\vec{\rho}), \tag{14}$$

where $\phi^{(+)}_{os}(\vec{p}_i,\vec{\rho})$ and $\phi^{(-)}_{os}(\vec{p}_j,\vec{\rho})$ are the lowest-lying harmonic oscillator states of the N-cluster and K-cluster given in the momentum space,

$$\phi^{(\pm)}_{os}(\vec{p}_i,\vec{\rho}) = (2\sqrt{\pi}b_i)^{3/2}\exp\left(-\frac{1}{2}b_i^2\vec{p}_i^{\,2} \mp i\lambda_{\pm}\vec{p}_i\cdot\vec{\rho}\right), \tag{15}$$

in which $\vec{\rho}$ is the vector representing the separation between the centers of mass of the two clusters and parameters $\lambda_{\pm}$ are defined by

$$\lambda_- = \beta_1 = \frac{3m_1}{4m_1+m_2}, \lambda_+ = \beta_2 = \frac{m_1+m_2}{4m_1+m_2}, \tag{16}$$

here m_1 denotes the mass of d and u quarks, and m_2 the mass of strange quark. The wave function in Eq. (14) can be represented through the cluster coordinates in the form

$$R(\vec{p}_1,\vec{p}_2,\vec{p}_3,\vec{p}_4,\vec{p}_5;\vec{\rho}) = X_K(\vec{q})X_N(\vec{k}_1,\vec{k}_2)\Gamma(\vec{Q},\vec{\rho})Z_{CM}(\vec{P}), \tag{17}$$

where $X_K(\vec{q})$ and $X_{\underline{N}}(\vec{k}_1\ \vec{k}_2)$ are the internal motion wave functions of the $K(\overline{K})$ cluster $(q\bar{s})$ $[(\bar{q}s)]$ and the N cluster (qqq), with $\vec{q}$ and $\vec{k}_1,\vec{k}_2$ being the relative momenta in the clusters $(q\bar{s})$ $[(\bar{q}s)]$ and (qqq) respectively, $\Gamma(\vec{Q},\vec{\rho})$ is the wave function describing the relative motion between the two clusters with $\vec{Q}$ being the relative momentum of the two clusters and $Z_{CM}(\vec{P})$ the wave function for the center-of-mass motion of the whole system in which $\vec{P}$ is the total momentum of the system. According to the RGM, the wave function of the two clusters may be represented in the form

$$\overline{\Psi}_{TM\ sm} = \int d^3\rho\Phi_{TM(1/2)m_s}(\vec{p}_1,\vec{p}_2,\vec{p}_3,\vec{p}_4,\vec{p}_5;\vec{\rho})f(\vec{\rho}), \tag{18}$$

where $\Phi_{TM(1/2)m_s}(\vec{p}_1,\vec{p}_2,\vec{p}_3,\vec{p}_4,\vec{p}_5;\vec{\rho})$ is the basis function defined in Eqs. (10) and (11) and $f(\vec{\rho})$ is the unknown function describing the relative motion of the two clusters. On substituting the above wave function in Eq. (1), according to the well-known procedure, one may derive a resonating group equation satisfied by the function $f(\vec{\rho})$. Then, by the following transformation

$$f(\vec{\rho}) = \int d^3R\Gamma(\vec{\rho},\vec{R})\overline{\Psi}(\vec{R}), \tag{19}$$

where

$$\Gamma(\vec{\rho},\vec{R}) = \frac{1}{\sqrt{2}(2\pi)^3}\left(\frac{3\beta_2}{\pi b^2}\right)^{3/4}\int d^3k e^{(1/6\beta_2)b^2\vec{k}^2+i\vec{k}\cdot(\vec{\rho}-\vec{R})}, \tag{20}$$

in which b is the harmonic oscillator size parameter, the resonating group equation will be transformed to the following Schrödinger equation satisfied by the relative motion of the two clusters:

$$-\frac{1}{2\mu}\nabla^2_{\vec{R}}\overline{\Psi}(\vec{R}) + \int d^3R' V(\vec{R},\vec{R}')\overline{\Psi}(\vec{R}') = \varepsilon\overline{\Psi}(\vec{R}), \tag{21}$$

where ε, μ, and $\overline{\Psi}(\vec{R})$ are, respectively, the energy of relative motion, the reduced mass, and the Schrödinger-type wave function for the two clusters and

$$V(\vec{R},\vec{R}') = V^t(\vec{R},\vec{R}') + V^s(\vec{R},\vec{R}') + V^c(\vec{R},\vec{R}') \tag{22}$$

is the nonlocal $KN(\overline{K}N)$ effective interaction potential in which $V^t(\vec{R},\vec{R}')$, $V^s(\vec{R},\vec{R}')$, and $V^c(\vec{R},\vec{R}')$ are generated by the t-channel OGEP, the s-channel OGEP, and the confining potential. The potential $V(\vec{R},\vec{R}')$ in the Schrödinger equation is connected with the potential $V(\vec{\rho},\vec{\rho}')$ appearing in the resonating group equation by the following formula:

$$V(\vec{R},\vec{R}') = \int d^3\rho d^3\rho'\ \Gamma(\vec{R},\vec{\rho})V(\vec{\rho},\vec{\rho}')\Gamma(\vec{\rho}',\vec{R}'), \tag{23}$$

where $V(\vec{\rho},\vec{\rho}')$ is described in Appendix B. To compute the elastic scattering phase shifts, we need to calculate the transition matrix between initial and final plane wave functions as follows

$$T_{fi}(\vec{k},\vec{k}') = \int d^3Rd^3R' e^{-i\vec{k}\cdot\vec{R}}V(\vec{R},\vec{R}')e^{i\vec{k}'\cdot\vec{R}'}, \tag{24}$$

where $\vec{k}'$ and $\vec{k}$ are the $KN(\overline{K}N)$ relative momenta for the initial and final states, respectively. Upon substituting Eq. (20) into Eq. (23), it is easy to find

$$T_{fi}(\vec{k},\vec{k}') = \frac{1}{2}\left(\frac{3\beta_2}{\pi b^2}\right)^{3/2}e^{(b^2/6\beta_2)(\vec{k}^2+\vec{k}'^2)} \times\int d^3\rho d^3\rho' e^{-i\vec{k}\cdot\vec{\rho}}V(\vec{\rho},\vec{\rho}')e^{i\vec{k}'\cdot\vec{\rho}'}. \tag{25}$$

This expression shows that to calculate the transition matrix, we may directly use the potential $V(\vec{\rho},\vec{\rho}')$ instead of the potential $V(\vec{R},\vec{R}')$.

III. CALCULATION OF PHASE SHIFTS

The phase shifts of the $KN(\bar{K}N)$ low-energy elastic scattering are calculated in the Born approximation. As argued in Appendix C and demonstrated in the previous literature (14) and (15), the Born approximation can reasonably describe hadron elastic low-energy scattering processes. In this approximation and in the center-of-mass frame, the lth partial wave phase shift is expressed by the following formula whose derivation will be sketched in Appendix C:

$$\delta_l^{IJ} = -2MkT_{fi}^{IJl}(k), \tag{26}$$

where

$$M(E) = \frac{E^4 - (m_K^2 - m_N^2)^2}{4E^3}, \tag{27}$$

in which E is the total energy of the $KN(\bar{K}N)$ system, m_K and m_N are the masses of kaon and nucleon, $k=|\vec{k}|=|\vec{k}'|$ is the magnitude of relative momenta $\vec{k}$ and $\vec{k}'$ in the case of elastic scattering, and $T_{fi}^{IJl}(k)$ with isospin I, total angular momentum J, and orbital angular momentum l is the transition amplitude. This amplitude can generally be expressed as

$$T_{fi}^{IJl}(k) = \sum_{m,m',\mu,\mu'} C_{lm'(1/2)m_s}^{JM} C_{lm(1/2)m_s'}^{JM} \times \int d\Omega(\hat{k}) d\Omega(\hat{k}') Y_{lm'}^{*}(\hat{k}') Y_{lm}(\hat{k}) T_{fi}^{I}(\vec{k}, \vec{k}'; m_s, m_s'), \tag{28}$$

where $C_{lm(1/2)m_s}^{JM}$ are the Clebsch-Gordan coefficients, $Y_{l\,m}(\hat{k})$ are the spherical harmonic functions, and

$$T_{fi}^{I}(\vec{k};\vec{k}', m_s, m_s') = \left\langle C; I, M; \tfrac{1}{2}, m_s | V_{f\,i}(\vec{k}, \vec{k}') | I, M_I; \tfrac{1}{2}, m_s'; C \right\rangle \tag{29}$$

are the matrix elements of the operator $V_{fi}(\vec{k}, \vec{k}')$ defined in Eq. (25) between the color-spin-isospin wave functions $|I, M_I; \frac{1}{2}, m_s'; C\rangle$ and $|I, M_I; \frac{1}{2}; m_s; C\rangle$ in which I, M_I and $\frac{1}{2}$, m_s are the isospin and spin quantum numbers of the $KN(\bar{K}N)$ system, respectively, and C denotes the color singlet of the whole system. These matrix elements can be easily calculated. The explicit expressions of the quantities $T_{fi}^{I}(\vec{k}, \vec{k}'; m_s, m_s')$ and $T_{f\,i}^{IJ\,l}(k)$, we think, are unnecessary to be listed in this paper. We only show here numerical results of the theoretical phase shifts in Figs. 1–6 using the conventional partial wave notation L_{I2J}. It is noted here that the formula in Eq. (28) is general for evaluating the transition amplitude, particularly, in the case where the spin-orbit coupling and tensor force terms are present in the nonlocal effective potentials.

We would like here to discuss the problem of suppression of the effect of spin-orbital coupling. It is a common recognition in the study of hadron spectroscopy that the effect of the spin-orbital coupling term in the t-channel OGEP ought to be suppressed by the corresponding term in the confining potential [2]. In Ref. [21], one of the authors in this paper and his co-workers proposed a $q\bar{q}$ confining potential which was obtained from a general Lorentz structure of the confinement. In the confining potential, there are various terms among which the spin-orbit coupling term is of a sign opposite to the corresponding one in the OGEP. In this paper, to avoid the complexity of such a confining potential, we alternatively take an effective treatment to achieve the spin-orbital suppression. Looking at the expression of the potential $V^t(\vec{\rho}, \vec{\rho}')$ shown in Appendix B, one can see that there is a kind of factorial functions to appear in some terms of the potential $V^t(\vec{\rho}, \vec{\rho}')$, which are of the form

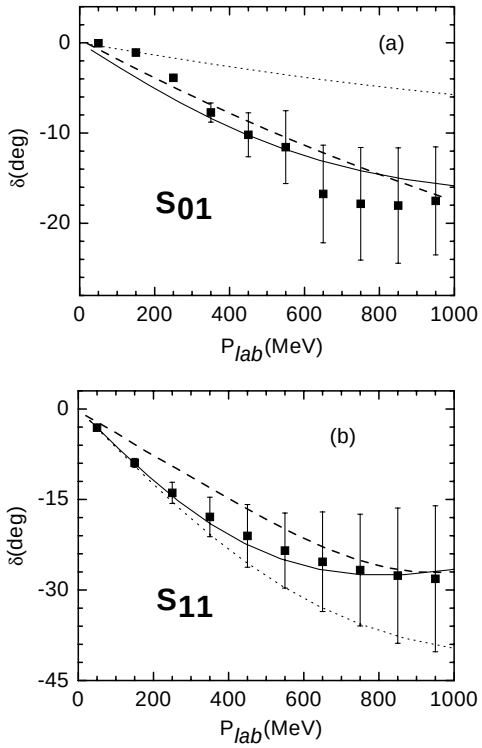

FIG. 1. The theoretical *KN* *S*-wave phase shifts in the I=0 and 1 channels. The solid lines represent the phase shifts by considering the effects of the color octet, the QCD renormalization, and the spin-orbit suppression. The dotted lines denote the result without considering the color octet and the dashed line shows the result without considering the QCD renormalization. The experimental phase shifts [29,30] are shown by black squares with error bars.

$$g(x, \vec{\rho}) = \int \frac{d^3r}{4\pi r} e^{-xr^2 + x\vec{r}\cdot\vec{\rho}}. \tag{30}$$

In particular, this function is related to the spin-orbit coupling term in the potential $V^t(\vec{\rho}, \vec{\rho}')$. The function $g(x, \vec{\rho})$ may appropriately be replaced by an interpolating function such that

$$g(x, \vec{\rho}) \simeq \frac{e^{(1-\gamma)(x\rho^2/4)}}{2\,x}. \tag{31}$$

To obtain the above expression, we have used the approximate expression of the following integral:

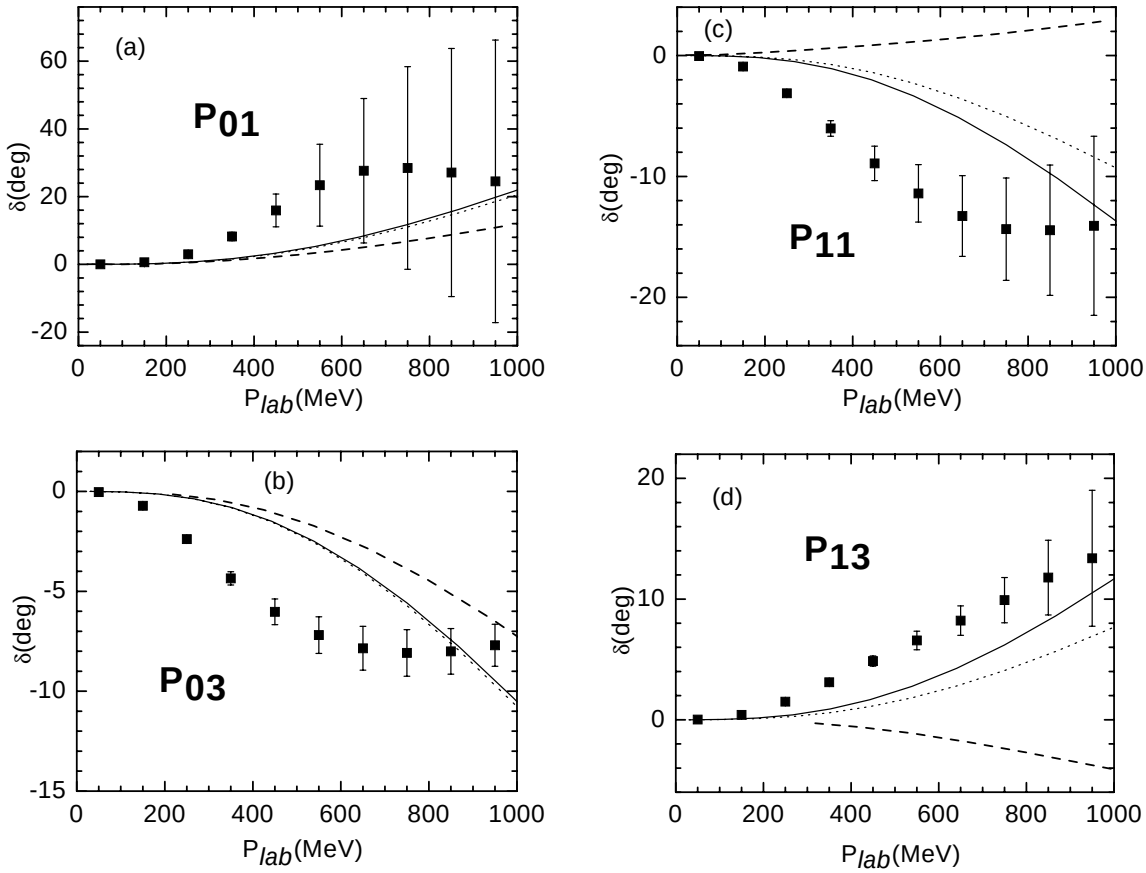

FIG. 2. The theoretical *KN P*-wave phase shifts in the $I=0$ and 1 channels. The solid lines represent the phase shifts by considering the effects of the color octet, the QCD renormalization, and the spin-orbit suppression. The dotted and dashed lines denote the results without considering the color octet and the QCD renormalization, respectively. The experimental phase shifts [29,30] are shown by black squares with error bars.

$$f(x) = \int_0^x e^{-t^2} dt \approx x e^{-\gamma x^2}. \tag{32}$$

As shown in Fig. 5, when we take the parameter $\gamma=0.3$, the function on the right hand side of Eq. (32) nearly approaches the real value of the integral when x is not too large. However, as shown in Fig. 6, the above value of γ leads to worse *P*-wave phase shifts. In order to get better *P*-wave phase shifts, we have to take some larger value of γ which just plays the role of suppressing the effect of spin-orbital coupling.

Finally, let us discuss the inclusion of QCD renormalization effect. As mentioned in the Introduction, the OGEP is derived from the *S* matrix or the BS irreducible interaction kernel in the tree diagram approximation. Obviously, to improve our calculation, it is natural to consider the correction arising from QCD renormalization. This can be done by replacing the QCD coupling constant and quark masses in the OGEP with the effective ones which are obtained by solving the renormalization group equations satisfied by the renormalized coupling constant and quark masses. This procedure, as proved in Ref. [27] and demonstrated in Appendix D, is equivalent to replacing the free wave functions, the free propagators and the bare vertices in the tree diagrams with the exact ones. In the calculation of this paper, we employ the effective coupling constant and quark masses given in Ref. [23] which were derived from QCD in the one-loop approximation and the mass-dependent momentum space subtraction. These effective quantities are suitable to any energy, particularly, to the low energy, unlike the results obtained in the minimal subtraction [28], which actually are applicable only in the large momentum limit. The effective fine structure constant used has the expression [23] like this:

$$\alpha_R(\lambda) = \frac{\alpha_R^0}{1 + \frac{\alpha_R^0}{2\pi} G(\lambda)}, \tag{33}$$

where α_R^0 is a coupling constant and $G(\lambda)$ is a function of variable λ which has different expressions given by the timelike momentum subtraction (the subtraction performed at timelike renormalization point) and the spacelike momentum subtraction (the subtraction carried out at the spacelike renormalization point). For the timelike momentum subtraction,

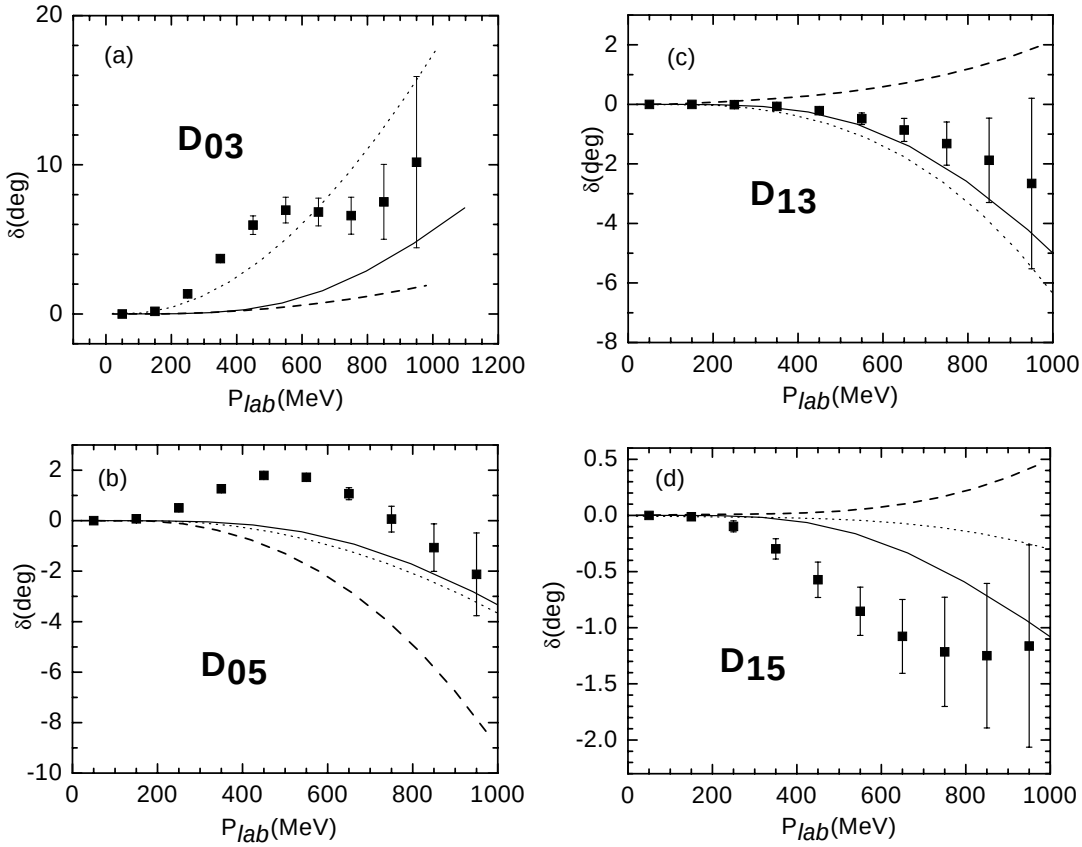

FIG. 3. The theoretical *KN D*-wave phase shifts in the $I=0$ and 1 channels. The solid lines represent the phase shifts by considering the effects of the color octet, the QCD renormalization, and the spin-orbit suppression. The dotted and dashed lines denote the results without considering the color octet and the QCD renormalization, respectively. The experimental phase shifts [29,30] are shown by black squares with error bars.

$$G(\lambda) = 11\ \ln\lambda - \frac{2}{3}N_f\left[2 + \sqrt{3}\pi - \frac{2}{\lambda^2} + \left(\frac{2}{\lambda^2}+1\right) \times \frac{\sqrt{\lambda^2-4}}{\lambda}\ln\frac{1}{2}(\lambda + \sqrt{\lambda^2-4})\right], \tag{34}$$

where N_f is the quark flavor number which will be taken to be 3 in this paper. While, for the spacelike momentum subtraction,

$$G(\lambda) = 11\ \ln\lambda - \frac{2}{3}N_f\left[\frac{2}{\lambda^2} - 2 - \left(\frac{2}{\lambda^2}-1\right)\frac{\sqrt{\lambda^2+4}}{\lambda} \times \ln\frac{1}{2}(\lambda + \sqrt{\lambda^2+4}) + \sqrt{5}\ln\frac{1}{2}(1+\sqrt{5})\right], \tag{35}$$

in which λ is defined as $\lambda = \sqrt{q^2/\mu^2}$ with q being a momentum variable and μ the fixed scale parameter. The expression in Eq. (33) with the function $G(\lambda)$ given either in Eq. (34) and (35) will immediately go over to the result given in the minimal subtraction in the large momentum limit. The latter subtraction was performed at the spacelike renormalization point. It would be noted that in writing the above effective coupling constant, the mass difference between different quarks is ignored for simplicity. The behaviors of the effective coupling constants given in Eqs. (33)–(35) are described in Fig. 7. From the figures, we see that the effective coupling constants given by the timelike and spacelike momentum subtractions have different behaviors in the low-energy regime. It is interesting to note that the effective coupling constant given in the spacelike momentum subtraction is almost the same as given in the minimal subtraction in the regime. This situation happens only in the case of ignoring the mass difference between different quarks and taking $N_f=3$. In other cases, the difference between the results given by the both subtractions will be manifest.

The effective quark mass is represented as

$$m_R(\lambda) = m_R e^{-S(\lambda)}, \tag{36}$$

where m_R is the constant quark mass given at $\lambda=1$ which will appropriately be chosen to be the constituent quark mass in the quark potential model, and $S(\lambda)$ is a function which also has different expressions for the different subtractions. For the timelike momentum subtraction,

$$S(\lambda) = \frac{\alpha_R^0}{\pi}\frac{1-\lambda}{\lambda}\left\{2 + \left(\frac{2}{\lambda^2} - \frac{1+\lambda}{\lambda^2}\right)\ln|1-\lambda^2|\right\}, \tag{37}$$

while, for the spacelike momentum subtraction,

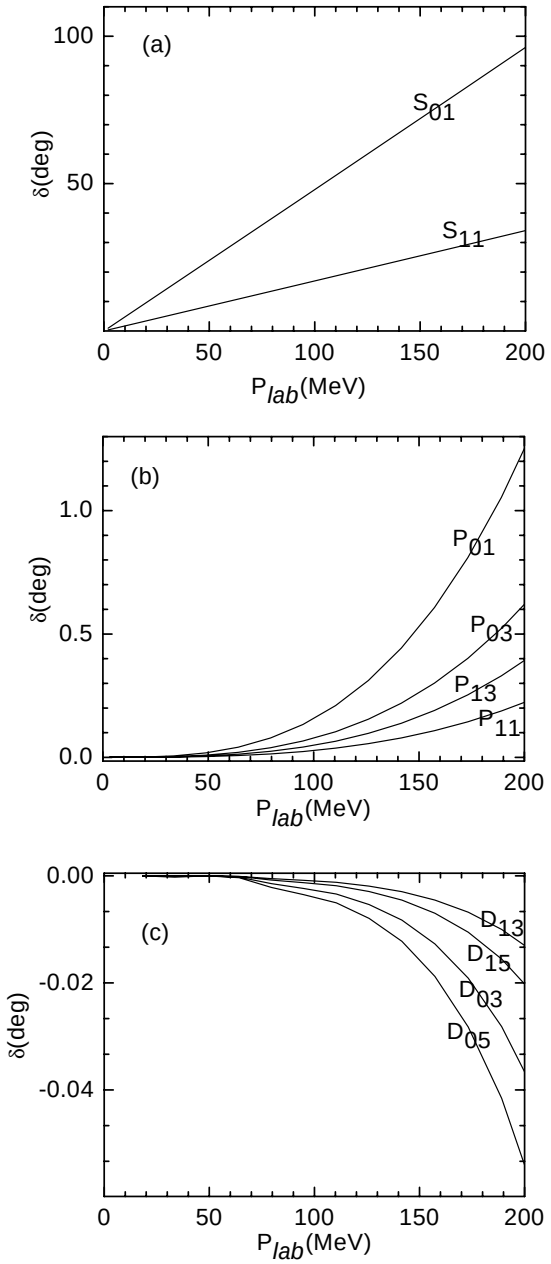

FIG. 4. The theoretical predictions for the $\bar{K}N$ *S*-, *P*-, and *D*-wave phase shifts.

$$S(\lambda) = S_1(\lambda) + iS_2(\lambda), \tag{38}$$

where

$$S_1(\lambda) = \frac{\alpha_R^0}{\pi}\left[\left(\frac{3}{\lambda^2}+1\right)\ln(1+\lambda^2) - 4\sqrt{2}\right] \tag{39}$$

and

$$S_2(\lambda) = \frac{2\alpha_R^0}{\pi}\left[\frac{1}{\lambda^3}\ln(1+\lambda^2) - \frac{1}{\lambda} + 1 - \ln\sqrt{2}\right]. \tag{40}$$

The behaviors of the effective quark mass given by the timelike momentum subtraction and the real part of the effective quark mass given in the spacelike momentum subtraction are depicted in Fig. 8. The figures show that at low energy the effective masses given in the both subtractions are not so much different. For the interaction taking place in the *t*-channel, as explained in Appendix D, the transfer momentum is spacelike, while for the interaction in the *s* channel, the transfer momentum is timelike. Therefore, for the *t*-channel OGEP, we will use the effective coupling constant and quark masses given by the

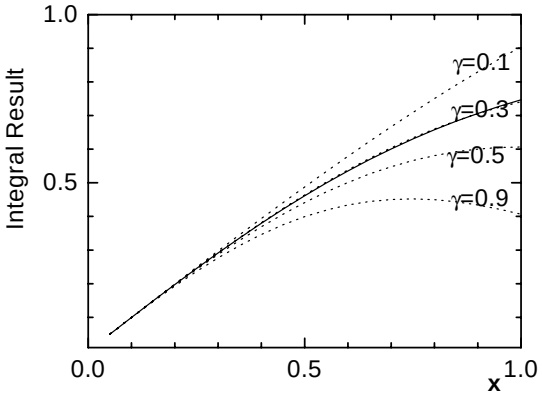

FIG. 5. The approximate expressions of the integral $f(x)$ in Eq. (32) given by different values of the parameter γ which are plotted with the dotted lines. The real values of the integral is represented by the solid line.

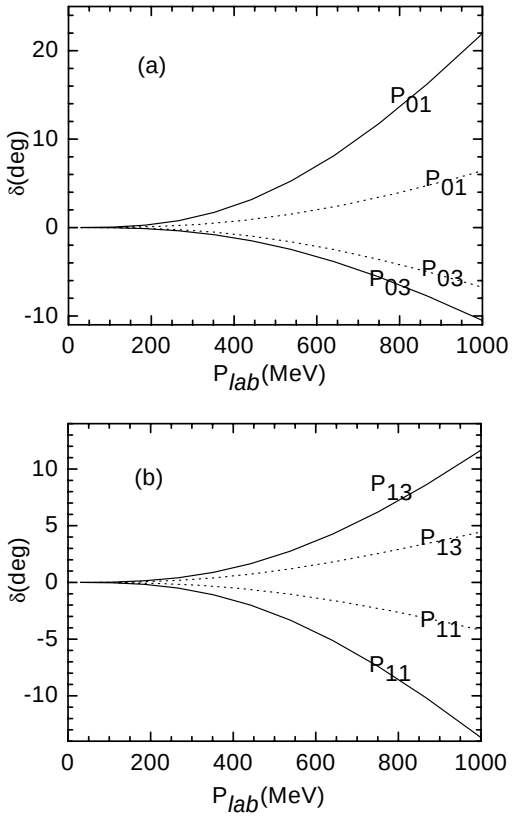

FIG. 6. Illustration of the effect of the spin-orbit suppression on the *P*-wave phase shifts. The solid lines represent the final results given by taking the parameter γ=0.45. The dotted lines denote the results given by γ=0.30.

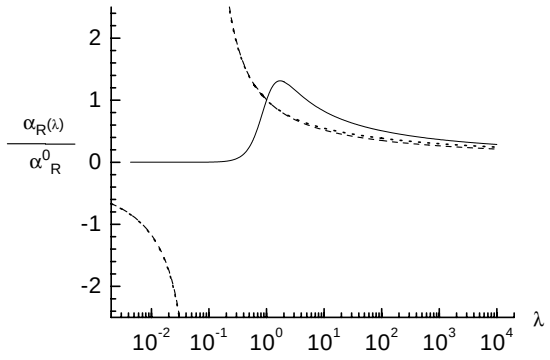

FIG. 7. The QCD effective coupling constants obtained from the one-loop renormalization. The solid, dashed, and dotted lines represent the results given by the timelike momentum subtraction, the spacelike momentum subtraction, and the minimal subtraction, respectively.

spacelike momentum subtraction and in this case, we only adopt the real part of the effective masses in our calculation; while, for the *s*-channel OGEP, the effective coupling constant and the quark masses given in the timelike momentum subtraction will be employed. The variable λ is usually defined as a ratio of the momentum related to the process of quark-gluon interactions. In this paper, as an effective treatment, we directly define it as $\lambda = k/\mu$ where k is taken to be the magnitude of the relative momentum of the two interacting particles K and N (or $\bar{K}$ and N).

IV. RESULTS AND DISCUSSIONS

This section is used to present calculated results for the $KN(\bar{K}N)$ elastic scattering phase shifts, discuss adjustments of the theoretical parameters, and analyze the effect of color octet and QCD renormalization as well as the suppression of the spin-orbital coupling. First, we focus our attention on the *KN* scattering. The theoretical phase shifts of the *KN* scattering are depicted in Figs. 1–3. In the figures, the solid lines represent the final results obtained by considering the contributions arising from the color octet, the QCD renormalization and the spin-orbit suppression. To exhibit the effects of the color octet and the QCD renormalization, in the figures, we also show the results without considering these effects. Such results are calculated with the same parameters as for the solid lines and represented by the dotted and dashed lines, respectively, in Figs. 1–3. The figures show us that the agreement between the final calculated results and the experimental data is good for the phase shifts of all *S* waves, P_{13} wave and D_{13} wave in the low-energy domain, particularly in the region of the laboratory momentum less than 600 MeV to which the nonrelativistic quark potential model is considered to be applicable. For the other *P*-wave and *D*-wave phase shifts, the agreement is qualitatively reasonable. In obtaining these results, we used the parameters as follows: the QCD coupling constant $\alpha_s^0 = 0.23$, the constituent quark masses $m_u = m_d = 350$ MeV and $m_s = 550$ MeV, the size parameter of harmonic oscillator ($b = 0.255$ fm), the force strength of confinement ($\omega = 0.2$ GeV), the color combination coefficient $\alpha = 0.915$, the scale parameter of QCD renormalization ($\mu = 0.195$ GeV), and the parameter of spin-orbital suppression ($\gamma = 0.45$). These parameters are adjusted to give a better fit to the *KN* elastic scattering experimental data, mainly to the *S*-wave phase shifts because the *KN* elastic scattering data are available and are rather sufficient [29,30]. In comparison with the previous results given in Refs. [10,11,17,18], our calculation achieves a considerable improvement on the theoretical phase shifts for all the partial waves not only in the magnitude, but also in the sign. Especially, for the P_{13}-wave phase shift, it now gets a right sign in our calculation, opposite to the previous result which was given a wrong sign [17].

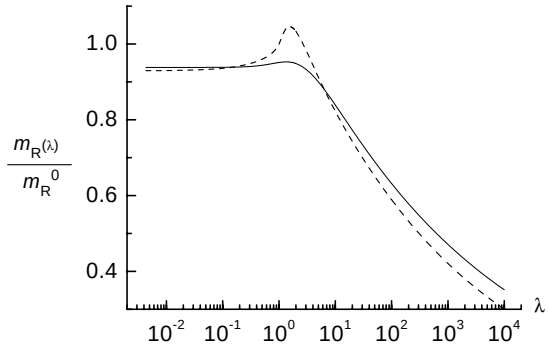

FIG. 8. The QCD effective quark masses obtained from the one-loop renormalization. The solid line represents the result given by the timelike momentum subtraction. The dashed line shows the real part of the effective quark mass given in the spacelike momentum subtraction.

Now let us analyze the effects of the color octet, the QCD renormalization and the suppression of the spin-orbital coupling. In adjusting the theoretical parameters, we found that the calculated results are sensitive to the parameters α and b. Any small change would cause noticeable influence on calculated values. For instance, when we let α increase, the absolute values of *S*-wave phase shifts decrease rather fast. In particular, when the α tends to unity, i.e., the color octet is absent, as denoted by the dotted lines in Fig. 1, we obtain the *S*-wave phase shifts similar to those given in Ref. [17]. In this case, certainly, we may give a better fit of the calculated result to the experimental one by adjusting the parameter b and others, but, we failed to simultaneously get a good result for another *S*-wave phase shift, as was demonstrated previously in Ref. [18]. Only when the color octet is considered, it is possible to get consistently good results for both the *S*-wave phase shifts as denoted by the solid lines in Fig. 1. This suggests that the introduction of the color octet is necessary in our calculation. From Figs. 2 and 3, we also see that the inclusion of the color octet gives a appreciable effect on the *P*- and *D*-wave phase shifts.

In this paper, the two kinds of spin-orbital terms in the *t*-channel OGEP, the spin-symmetric term and the spin-antisymmetric one, are all taken into account. In this case, we still encountered the puzzling problem for the *P*-wave phase shifts as was revealed originally in Ref. [11] and mentioned in the Introduction. If the QCD renormalization effect

is not considered, except for the P_{11}- and P_{13}-wave phase shifts, it seems to be able to reproduce the phase shifts for the other phase shifts by readjusting the parameters involved. However, as exhibited in Fig. 2, for the P_{11} and P_{13} waves, it is impossible to get a satisfactory result of their phase shifts. Particularly, for the P_{13} wave, its phase shift is always of a wrong sign as the previous result given in Ref. [17]. This problem can only be resolved by taking the QCD renormalization effect into account in our calculation. In this way, the P_{11}- and P_{13}-wave phase shifts are accessible to the experimental values. As shown in Fig. 3, the QCD renormalization effect gives an essential improvement on the *D*-wave phase shifts as well. Particularly, it renders the D_{13}- and D_{15}-wave phase shifts to have the right signs. But, this effect is not noteworthy for the *S*-wave phase shifts. This explains why the previous investigations could give some rather reasonable results for the *S*-wave phase shift. However, as shown in our calculation, in order to get the desirable phase shifts for all partial waves, it is necessary to incorporate the QCD renormalization effect into the model used. In addition, to achieve such results, as mentioned in Sec. III, the spin-orbital coupling effect is necessary to be suppressed. The necessity of the suppression is separately illustrated in Fig. 6 for the *P*-wave phase shifts only. This is because the spin-orbit term in the effective potential gives no contribution to the *S*-wave scattering and it mainly affects the *P*-wave scattering. Figure 6 indicates that when the parameter γ is taken to be the value $\gamma=0.3$, which makes the function $g(x,\vec{\rho})$ reach its real values, the P_{01}-wave and the P_{11} wave phase shifts are far from the experimental ones, but, when the γ is getting larger, the absolute values of the P_{01} wave and the P_{11} wave phase shifts become comparable with the experimental results. For the other *P*-waves, the phase shifts evaluated at $\gamma=0.45$ are also better than those given at $\gamma=0.3$.

Let us turn to the $\bar{K}N$ scattering. At present, the low-energy elastic and inelastic experimental data for the $\bar{K}N$ scattering are insufficient [31–33]. Therefore, the detailed partial wave analysis for the scattering is almost absent. But it is a common conclusion suggested in the previous investigations that the $K^- p$ interaction is strongly attractive [34]. For the $\bar{K}N$ scattering in the $I=1$ channel, i.e., for the K^--neutron scattering, there are almost no available data and different theoretical models give different predictions [35,36]. In view of this situation, our calculated results for the $\bar{K}N$ phase shifts can only be viewed as a theoretical prediction. It would be noted that unlike the *KN* interaction for which the exchanged part of the effective potential generated from the *t*-channel OGEP is dominant, for the $\bar{K}$-*N* interaction, there is no such exchange potential. Instead, the direct part of the *s*-channel OGEP plays an essential role and leads to an attractive interaction as seen from the positiveness of the phase shifts plotted in Fig. 4. In the figure, the prediction for the *P*- and *D*-wave phase shifts are simultaneously given as well. All the phase shifts in the figure are presented in the momentum region less than 200 MeV where any resonance could not appear. Here we take the $K^- p$ *S*-wave phase shift given in this paper as an example to estimate the reasonability of our calculation. From the relation $\sqrt{\pi}|a^l_{eff}| \simeq |f^l_+|$ (Ref. [37]), where a^l_{eff} is the effective scattering length and f^l_+ is the *l*th wave scattering amplitude, and the formulas given in Eq. (C2) and (C15), we have $\delta^{IJ}_l \simeq kRe(a^l_{eff})$. By this relation and the calculated *S*-wave phase shift, it is found that the real part of the scattering length is above 0.58, which just lies in the range shown in Refs. [33,35]. In addition, we note that our calculation predicts a weaker attraction for the K^--neutron interaction which is different from the previous result (see Ref. [39]).

At last, it should be emphasized that the quark potential model used in this paper was established in the nonrelativistic approximation of order p^2/m^2, therefore, the calculated results are only valid for the *KN* and $\bar{K}N$ elastic scattering in the low-energy domain. The model used cannot give a complete description for the inelastic scattering and the production of resonances which would appear for some higher-partial waves in the higher-energy regime. To explore the *KN* and $\bar{K}N$ inelastic scattering in the higher energy regime, it is necessary to apply a relativistic approach or a nonperturbative theory. Anyway, the investigation based on the constituent quark model is meaningful as it is not only helpful to understand *KN* and $\bar{K}N$ interactions from the underlying dynamics, but also provides a firm basis of studying five-quark bound states.

ACKNOWLEDGMENTS

The authors would like to express their thanks to Professor Dick Arndt for his kind help. He offered us the experimental data which are useful in our calculation. This project was supported in part by the National Natural Science Foundation of China.

APPENDIX A: THE COLOR-FLAVOR-SPIN WAVE FUNCTIONS

In general, the color singlet color state of the five-quark cluster ($q^4\bar{s}$) or ($q^3\bar{q}s$) may be built up by the color singlets of the *N* cluster (*qqq*) and *K* cluster ($q\bar{s}$) [or the $\bar{K}$ cluster ($\bar{q}s$)] or the color octets of the two subclusters. Correspondingly, for the five-quark cluster, there are two classes of color-flavor-spin wave functions denoted by $\Psi^{(1)}_{TM(1/2)m}(1,2,3,4,5)$ and $\Psi^{(2)}_{TM(1/2)m}(1,2,3,4,5)$ which are color singlets as a whole, but associated, respectively, with the color singlets and the color octets of the two subclusters. In the function $\Psi^{(1)}_{TM(1/2)m}(1,2,3,4,5)$, the color-flavor-spin (CFS) wave function $\Psi^{(1)}_{(1/2)M_1(1/2)m_s}(1,2,3)_N$ for the *N* cluster which is totally antisymmetric (of the symmetry denoted by the Young diagram $[1^3]_{\rm CFS}$) is constructed from the $C-G$ coupling of $[1^3]_C \times [3]_{FS}$ where $[1^3]_C$ and $[3]_{FS}$ are the Young diagrams denoting the antisymmetric color singlet and the symmetric flavor-spin states, respectively. In the function $\Psi^{(2)}_{TM(1/2)m} \times (1,2,3,4,5)$, the antisymmetric CFS wave function $\Psi^{(1)}_{(1/2)M_1(1/2)m_s}(1,2,3)_N$ for the *N*-cluster is given by the $C-G$ coupling of $[21]_C \times [21]_{FS}$ where $[21]_C$ and $[21]_{FS}$ represent the color octet state and the flavor-spin state of mixed symmetry, respectively. The explicit expressions of the wave

functions mentioned above can easily be written out by the familiar method given in the group theory, as displayed in the following.

The first class of the CFS wave function in Eq. (12) for the whole system is

$$\Psi^{(1)}_{TM(1/2)m}(1,2,3,4,5) = \sum_{M_1M_2} C^{TM}_{(1/2)M_1(1/2)M_2}\Psi^{(1)}_{(1/2)M_1(1/2)m} \times (1,2,3)_N\Psi^{(1)}_{(1/2)M_200}(4,5)_K \tag{A1}$$

where $\Psi^{(1)}_{(1/2)M_1(1/2)m}(1,2,3)_N$, as mentioned before, is the CFS wave function for the N cluster and $\Psi^{(1)}_{(1/2)M_200}(4,5)_K$ is the CFS wave function for the K cluster. They are represented separately as

$$\Psi^{(1)}_{(1/2)M_1(1/2)m_s}(1,2,3)_N = \xi^0_c(1,2,3)\chi^{(1)}_{(1/2)M_1(1/2)m_s}(1,2,3), \tag{A2}$$

where

$$\xi^0_c(1,2,3) = \frac{1}{\sqrt{6}}\epsilon_{abc}q^a(1)q^b(2)q^c(3) \tag{A3}$$

represents the color singlet wave function of the N cluster and

$$\chi^{(1)}_{(1/2)M_1(1/2)m_s}(1,2,3) = \frac{1}{\sqrt{2}}[\chi^a_{(1/2)M_1}(1,2,3)\varphi^a_{(1/2)m_s}(1,2,3) + \chi^b_{(1/2)M_1}(1,2,3)\varphi^b_{(1/2)m_s}(1,2,3)] \tag{A4}$$

is the isospin-spin wave function of the N cluster in which the isospin wave functions $\chi^a_{(1/2)M_1}(1,2,3)$ and $\chi^b_{(1/2)M_1}(1,2,3)$ and the spin wave functions $\varphi^a_{(1/2)m_s}(1,2,3)$ and $\varphi^a_{(1/2)m_s}(1,2,3)$ are expressed as follows

$$\chi^a_{(1/2)M_1}(1,2,3) = \sum_{m,m_3,m_1,m_2} C^{(1/2)M_1}_{1m(1/2)m_3}C^{1m}_{(1/2)m_1(1/2)m_2} \times \chi_{(1/2)m_1}(1)\chi_{(1/2)m_2}(2)\chi_{(1/2)m_3}(3),$$

$$\chi^b_{(1/2)M_1}(1,2,3) = \sum_{m_1,m_2,m_3} C^{(1/2)M_1}_{00(1/2)M_1}C^{00}_{(1/2)m_1(1/2)m_2} \times\chi_{(1/2)m_1}(1)\chi_{(1/2)m_2}(2)\chi_{(1/2)m_3}(3),$$

$$\varphi^a_{(1/2)m_s}(1,2,3) = \sum_{m,m_3,m_1,m_2} C^{(1/2)m_s}_{1m(1/2)m_3}C^{1m}_{(1/2)m_1(1/2)m_2} \times \varphi_{(1/2)m_2}(1)\varphi_{(1/2)m_2}(2)\varphi_{(1/2)m_3}(3),$$

$$\varphi^b_{(1/2)m_s}(1,2,3) = \sum_{m_1,m_2,m_3} C^{(1/2)m_s}_{00(1/2)m_s}C^{00}_{(1/2)m_1(1/2)m_2} \times\varphi_{(1/2)m_2}(1)\varphi_{(1/2)m_2}(2)\varphi_{(1/2)m_3}(3). \tag{A5}$$

The CFS wave function of the K cluster is

$$\Psi^{(1)}_{(1/2)M00}(4,5)_K = C_0(4,5)\chi_{(1/2)M}(4,5)\varphi_{00}(4,5) \tag{A6}$$

where $C_0(4,5)$, $\chi_{(1/2)M}(4,5)$, and $\varphi_{00}(4,5)$ are the color, isospin, and spin wave functions, respectively. Since there are no identical particles in the cluster, these wave functions are of the forms

$$C_0(4,5) = \frac{1}{\sqrt{3}}q^a(4)\bar{q}^a(5) \tag{A7}$$

and

$$\chi_{(1/2)M}(4,5) = \sum_{m_1\ m_2} C^{(1/)2M}_{(1/2)m_100}\chi_{(1/2)m_1}(4)\chi_{00}(5),$$

$$\varphi_{00}(4,5) = \sum_{m_1\ m_2} C^{00}_{(1/2)m_1(1/2)m_2}\varphi_{(1/2)m_1}(4)\varphi_{(1/2)m_2}(5) \tag{A8}$$

For the second class of the CFS wave function in Eq. (12), it can be represented as

$$\Psi^{(2)}_{TM(1/2)m}(1,2,3,4,5) = \sum_{M_1M_2}\sum_c C^{TM_T}_{(1/2)M_1(1/2)M_2}\Psi^{(2)c}_{(1/2)M_1(1/2)m}(1,2,3)_N \times\Psi^{(2)c}_{(1/2)M00}(4,5)_K, \tag{A9}$$

where $\Psi^{(2)c}_{(1/2)M_1(1/2)m}(1,2,3)_N$ and $\Psi^{(2)c}_{(1/2)M00}(4,5)_K$ are the second class of CFS wave functions for the N cluster and the K cluster, respectively. Their expressions are shown in the following.

$$\Psi^{(2)C}_{(1/2)M_1(1/2)m_s}(1,2,3)_N = \frac{1}{\sqrt{2}}[\xi^A_c(1,2,3)\chi^{(2)B}_{(1/2)M_1(1/2)m_s}(1,2,3) - \xi^B_c(1,2,3)\chi^{(2)A}_{(1/2)M_1(1/2)m_s}(1,2,3)], \tag{A10}$$

where $\xi^A_c(1,2,3)$ and $\xi^B_c(1,2,3)$ are the color octet wave functions given, respectively, by the Young-Tableau [211] and [121], and $\chi^{(2)A}_{(1/2)M_1(1/2)m_s}(1,2,3)$ and $\chi^{(2)B}_{(1/2)M_1(1/2)m_s}(1,2,3)$ are the corresponding isospin-spin wave functions. Their expressions are

$$\xi^A_c(1,2,3) = (1/2)\epsilon_{ijb}[q^a(1)q^i(2)q^j(3) + q^a(2)q^i(1)q^j(3)],$$

$$\xi^B_c(1,2,3) = (1/2\sqrt{3})\epsilon_{ijb}[q^a(1)q^i(2)q^j(3) - q^a(2)q^i(1)q^j(3) - 2q^a(3)q^i(1)q^j(2)],$$

$$\chi^{(2)A}_{(1/2)M_1(1/2)m_s}(1,2,3) = (1/\sqrt{2}) \times[\chi^{a}_{(1/2)M_1}(1,2,3)\varphi^{a}_{(1/2)m_s}(1,2,3) - \chi^{b}_{(1/2)M_1}(1,2,3)\varphi^{b}_{(1/2)m_s}(1,2,3)],$$

$$\chi^{(2)B}_{(1/2)M_1(1/2)m_s}(1,2,3) = -(1/\sqrt{2}) \times[\chi^{a}_{(1/2)M_1}(1,2,3)\varphi^{b}_{(1/2)m_s}(1,2,3) + \chi^{b}_{(1/2)M_1}(1,2,3)\varphi^{a}_{(1/2)m_s}(1,2,3)]. \quad \text{(A11)}$$

The second class of the CFS wave function for the K(or $\bar{K}$) cluster is as follows:

$$\Psi^{(2)c}_{(1/2)M00}(4,5)_{\pi} = C^{b}_{a}(4,5)\chi_{(1/2)M}(4,5)\varphi_{00}(4,5), \quad \text{(A12)}$$

where

$$C^{b}_{a}(4,5) = q^{b}(4)q_{a}(5) - \frac{1}{3}\delta^{b}_{a}q^{c}(4)q_{c}(5) \quad \text{(A13)}$$

is the color octet for the $K(\bar{K})$ cluster and the other two functions $\chi_{(1/2)M}(4,5)$, $\varphi_{00}(4,5)$ are the same as in Eq. (A8).

APPENDIX B: THE EFFECTIVE *KN* AND $\bar{K}N$ INTERACTION POTENTIALS

In this appendix, we show the nonlocal effective interaction potentials of the *KN* and $\bar{K}N$ systems which are derived from the interquark potentials and the RGM.

The *KN* nonlocal effective potential $V_t(\vec{\rho},\vec{\rho}')$ which is derived from the *t*-channel OGEP written in Eq. (4) is divided into two parts: the direct part $V^{D}_{t}(\vec{\rho},\vec{\rho}')$ and the exchanged part $V^{ex}_{t}(\vec{\rho},\vec{\rho}')$:

$$V_t(\vec{\rho},\vec{\rho}') = V^{D}_{t}(\vec{\rho},\vec{\rho}') - V^{t}_{ex}(\vec{\rho},\vec{\rho}'), \quad \text{(B1)}$$

where

$$V^{ex}_{t}(\vec{\rho},\vec{\rho}') = V^{ex}_{t}(\vec{\rho},\vec{\rho}')^{14} + V^{ex}_{t}(\vec{\rho},\vec{\rho}')^{24} + V^{ex}_{t}(\vec{\rho},\vec{\rho}')^{34}, \quad \text{(B2)}$$

here the superscript ab=14, 24, or 34 designates which pair of quarks interchange. Each part of the potential contains several terms as shown in the following:

$$V^{D}_{t}(\vec{\rho},\vec{\rho}') = V^{D}_{15}(\vec{\rho},\vec{\rho}') + V^{D}_{25}(\vec{\rho},\vec{\rho}') + V^{D}_{35}(\vec{\rho},\vec{\rho}') + V^{D}_{14}(\vec{\rho},\vec{\rho}') + V^{D}_{24}(\vec{\rho},\vec{\rho}') + V^{D}_{34}(\vec{\rho},\vec{\rho}'), \quad \text{(B3)}$$

$$V^{ex}_{t}(\vec{\rho},\vec{\rho}')^{ab} = V^{ex}_{14}(\vec{\rho},\vec{\rho}')^{ab} + V^{ex}_{24}(\vec{\rho},\vec{\rho}')^{ab} + V^{ex}_{34}(\vec{\rho},\vec{\rho}')^{ab} + V^{ex}_{12}(\vec{\rho},\vec{\rho}')^{ab} + V^{ex}_{23}(\vec{\rho},\vec{\rho}')^{ab} + V^{ex}_{15}(\vec{\rho},\vec{\rho}')^{ab} + V^{ex}_{25}(\vec{\rho},\vec{\rho}')^{ab} + V^{ex}_{35}(\vec{\rho},\vec{\rho}')^{ab} + V^{ex}_{45}(\vec{\rho},\vec{\rho}')^{ab} + V^{ex}_{13}(\vec{\rho},\vec{\rho}')^{ab}, \quad \text{(B4)}$$

the subscript in each term on the right hand sides (RHS) of Eqs. (B3) and (B4) marks the two interacting quarks: one in the N cluster and another in the K cluster. The terms $V^{D}_{ij}(\vec{\rho},\vec{\rho}')$ and $V^{ex}_{ij}(\vec{\rho},\vec{\rho}')^{ab}$ are derived by the RGM in such a way,

$$V^{D}_{ij}(\vec{\rho},\vec{\rho}') = \int \prod_{k=1}^{5} \frac{d\vec{p}_k}{(2\pi)^3}\frac{d\vec{p}'_k}{(2\pi)^3}\langle R(\vec{p}_1,\vec{p}_2,\vec{p}_3,\vec{p}_4,\vec{p}_5;\vec{\rho}) \times|V^{t}_{ij}|R(\vec{p}'_1,\vec{p}'_2,\vec{p}'_3,\vec{p}'_4,\vec{p}'_5;\vec{\rho}')\rangle \quad \text{(B5)}$$

and

$$V^{ex}_{ij}(\vec{\rho},\vec{\rho}')^{ab} = \int \prod_{i=1}^{5} \frac{d\vec{p}_k}{(2\pi)^3}\frac{d\vec{p}'_k}{(2\pi)^3}\langle R(\vec{p}_1,\vec{p}_2,\vec{p}_3,\vec{p}_4,\vec{p}_5;\vec{\rho}) \times|V^{t}_{ij}P_{ab}|R(\vec{p}'_1,\vec{p}'_2,\vec{p}'_3,\vec{p}'_4,\vec{p}'_5;\vec{\rho}')\rangle, \quad \text{(B6)}$$

where the quark potential V^{t}_{ij} was denoted in Eq. (4) and the position space wave function was given in Eq. (14).

First we describe the ten terms on the RHS of Eq. (B4). By introducing the following functions:

$$g(x,\vec{\rho}) = \int \frac{d^3r}{4\pi r}e^{-xr^2+x\vec{r}\cdot\vec{\rho}},$$

$$f^{t}_{24}(\vec{\rho},\vec{\rho}')_{ex} = e^{-(\vec{\rho}\cdot\vec{\rho}'/2b^2)-(\vec{\rho}^2/8b^2)-(3\beta_2/4b^2)(\vec{\rho}-\vec{\rho}')^2},$$

$$f^{t}_{25}(\vec{\rho},\vec{\rho}')_{ex} = e^{-(\vec{\rho}\cdot\vec{\rho}'/2b^2)-(\alpha_2/4b^2)(\vec{\rho}+\vec{\rho}')^2-(3\beta_2/4b^2)(\vec{\rho}-\vec{\rho}')^2},$$

$$f^{t}_{15}(\vec{\rho},\vec{\rho}')_{ex} = e^{-(\vec{\rho}\cdot\vec{\rho}'/2b^2)-(\alpha_2/4b^2)\vec{\rho}^2-(3\beta_2/4b^2)(\vec{\rho}-\vec{\rho}')^2},$$

$$f^{t}_{14}(\vec{\rho},\vec{\rho}')_{ex} = e^{-(\vec{\rho}\cdot\vec{\rho}'/2b^2)-(1/8b^2)(\vec{\rho}-\vec{\rho}')^2-(3\beta_2/4b^2)(\vec{\rho}-\vec{\rho}')^2},$$

$$f^{t}_{23}(\vec{\rho},\vec{\rho}')_{ex} = e^{-(\vec{\rho}\cdot\vec{\rho}'/2b^2)-(3\beta_2/4b^2)(\vec{\rho}-\vec{\rho}')^2}, \quad \text{(B7)}$$

the exchanged terms of the potential $V^{ex}_{t}(\vec{\rho},\vec{\rho}')^{14}$ can be written as

$$V^{ex}_{24}(\vec{\rho},\vec{\rho}')^{14} = \frac{4\pi\alpha_s C^{t}_{24}}{(2\pi b^2)^{3/2}}f^{t}_{24}(\vec{\rho},\vec{\rho}')_{ex}\left\{g\left(\frac{1}{2b^2},\vec{\rho}'\right) - \frac{1}{4m_1^2}(1+\vec{\sigma}_2\cdot\vec{\sigma}_4) - \frac{1}{4m_1^2b^2}\left[\frac{\vec{\rho}^2}{4b^2} - \frac{1}{b^2}\left(\frac{2\beta_2-1}{2}\vec{\rho}-\beta_2\vec{\rho}'\right)^2 - (1/2)\vec{\sigma}_2\cdot\vec{\sigma}_4 + i\frac{\beta_2}{8b^2}(1+\gamma)(\vec{\rho}\times\vec{\rho}')\cdot(\vec{\sigma}_2-\vec{\sigma}_4) + \frac{1}{16b^2}(1+\gamma^2)\vec{\rho}\cdot\vec{\sigma}_2\vec{\rho}\cdot\vec{\sigma}_4\right]g\left(\frac{1}{2b^2},\vec{\rho}\right)\right\}, \quad \text{(B8)}$$

$$V_{34}^{ex}(\vec{\rho},\vec{\rho}')^{14}=\frac{4\pi\alpha_s C_{34}^t}{(2\pi b^2)^{3/2}}f_{24}^t(\vec{\rho},\vec{\rho}')_{ex}\Bigg\{g\left(\frac{1}{2b^2},\vec{\rho}\right)-\frac{1}{4m_1^2}(1+\vec{\sigma}_3\cdot\vec{\sigma}_4)-\frac{1}{4m_1^2b^2}\Bigg[\frac{\vec{\rho}^2}{4b^2}-\frac{1}{b^2}\left(\frac{2\beta_2-1}{2}\vec{\rho}-\beta_2\vec{\rho}'\right)^2-(1/2)\vec{\sigma}_3\cdot\vec{\sigma}_4$$
$$+i\frac{\beta_2}{8b^2}(1+\gamma)(\vec{\rho}\times\vec{\rho}')\cdot(\vec{\sigma}_3-\vec{\sigma}_4)+\frac{1}{16b^2}(1+\gamma^2)\vec{\rho}\cdot\vec{\sigma}_3\vec{\rho}\cdot\vec{\sigma}_4\Bigg]g\left(\frac{1}{2b^2},\vec{\rho}\right)\Bigg\}, \tag{B9}$$

$$V_{14}^{ex}(\vec{\rho},\vec{\rho}')^{14}=\frac{4\pi\alpha_s C_{14}^t}{(2\pi b^2)^{3/2}}f_{14}^t(\vec{\rho},\vec{\rho}')_{ex}\Bigg\{g\left(\frac{1}{2b^2},\vec{\rho}-\vec{\rho}'\right)-\frac{1}{4m_1^2}(1+\vec{\sigma}_1\cdot\vec{\sigma}_4)-\frac{1}{4m_1^2b^2}\Bigg[-\frac{(\beta_2-\beta_1)^2}{4b^2}(\vec{\rho}-\vec{\rho}')^2+\frac{(\vec{\rho}+\vec{\rho}')^2}{b^2}-9$$
$$-\frac{1}{2}\vec{\sigma}_1\cdot\vec{\sigma}_4+i\frac{1}{b^2}(1+\gamma)(\vec{\rho}\times\vec{\rho}')\cdot(\vec{\sigma}_1+\vec{\sigma}_4)+\frac{1}{16b^2}(1+\gamma^2)(\vec{\rho}-\vec{\rho}')\cdot\vec{\sigma}_1(\vec{\rho}-\vec{\rho}')\cdot\vec{\sigma}_4\Bigg]g\left(\frac{1}{2b^2},\vec{\rho}-\vec{\rho}'\right)\Bigg\}, \tag{B10}$$

$$V_{12}^{ex}(\vec{\rho},\vec{\rho}')^{14}=\frac{4\pi\alpha_s C_{12}^t}{(2\pi b^2)^{3/2}}f_{24}^t(\vec{\rho}',\vec{\rho})_{ex}\Bigg\{g\left(\frac{1}{2b^2},\vec{\rho}'\right)-\frac{1}{4m_1^2}(1+\vec{\sigma}_1\cdot\vec{\sigma}_2)-\frac{1}{4m_1^2b^2}\Bigg[\frac{\vec{\rho}'^2}{4b^2}-\frac{1}{b^2}\left(\frac{2\beta_2-1}{2}\vec{\rho}'-\beta_2\vec{\rho}'\right)^2-\frac{1}{2}\vec{\sigma}_1\cdot\vec{\sigma}_2$$
$$+i\frac{\beta_2}{8b^2}(1+\gamma)(\vec{\rho}'\times\vec{\rho})\cdot(\vec{\sigma}_1-\vec{\sigma}_2)+\frac{1}{16b^2}(1+\gamma^2)\vec{\rho}'\cdot\vec{\sigma}_1\vec{\rho}'\cdot\vec{\sigma}_2\Bigg]g\left(\frac{1}{2b^2},\vec{\rho}'\right)\Bigg\}, \tag{B11}$$

$$V_{13}^{ex}(\vec{\rho},\vec{\rho}')^{14}=\frac{4\pi\alpha_s C_{13}^t}{(2\pi b^2)^{3/2}}f_{24}^t(\vec{\rho}',\vec{\rho})_{ex}\Bigg\{g\left(\frac{1}{2b^2},\vec{\rho}'\right)-\frac{1}{4m_1^2}(1+\vec{\sigma}_1\cdot\vec{\sigma}_3)-\frac{1}{b^2}\left(\frac{2\beta_2-1}{2}\vec{\rho}'-\beta_2\vec{\rho}\right)^2-\frac{1}{2}\vec{\sigma}_1\cdot\vec{\sigma}_3$$
$$+i\frac{\beta_2}{8b^2}(1+\gamma)(\vec{\rho}'\times\vec{\rho})\cdot(\vec{\sigma}_1-\vec{\sigma}_3)+\frac{1}{16b^2}(1+\gamma^2)\vec{\rho}'\cdot\vec{\sigma}_1\vec{\rho}'\cdot\vec{\sigma}_3\Bigg]g\left(\frac{1}{2b^2},\vec{\rho}'\right), \tag{B12}$$

$$V_{23}^{ex}(\vec{\rho},\vec{\rho}')^{14}=\frac{4\pi\alpha_s C_{23}^t}{(2\pi b^2)^{3/2}}f_{23}^t(\vec{\rho},\vec{\rho}')_{ex}\Bigg[b^2-\frac{1}{4m_1^2}-\frac{\vec{\sigma}_2\cdot\vec{\sigma}_3}{6m_1^2}+\frac{\beta_2^2}{4m_1^2b^2}(1+\gamma^2)(\vec{\rho}-\vec{\rho}')^2\Bigg], \tag{B13}$$

$$V_{15}^{ex}(\vec{\rho},\vec{\rho}')^{14}=\frac{4\pi\alpha_s C_{15}^t}{(\pi b^2/\alpha_1)^{3/2}}f_{15}^t(\vec{\rho},\vec{\rho}')_{ex}\Bigg\{g\left(\frac{\alpha_2}{b^2},\vec{\rho}\right)-\left(\frac{m_1^2+m_2^2}{8m_1^2m_2^2}+\frac{\vec{\sigma}_1\cdot\vec{\sigma}_5}{4m_1m_2}\right)-\frac{1}{4(m_1+m_2)^2b^2}\Bigg[\frac{6}{\alpha_1}-\frac{(\alpha_1\vec{\rho}-\beta_1\vec{\rho}+\beta_1\vec{\rho}')^2}{\alpha_1^2b^2}$$
$$-\frac{\alpha_2\beta_1}{4\alpha_1b^2}i(1-\gamma)(\vec{\rho}\times\vec{\rho}')\cdot\left[\left(1+\frac{m_2}{m_1}\right)\vec{\sigma}_1-\left(1+\frac{m_1}{m_2}\right)\vec{\sigma}_5\right]\Bigg]g\left(\frac{\alpha_2}{b^2},\vec{\rho}\right)-\frac{1}{4m_1m_2b^2}\Bigg[6\alpha_2-\frac{\alpha_2(\alpha_1-\alpha_2)\beta_1}{\alpha_1b^2}\vec{\rho}\cdot\vec{\rho}'$$
$$-\frac{\alpha_2(\alpha_1-\beta_1)^2-\alpha_2\beta_1\beta_2}{\alpha_1b^2}\vec{\rho}^2-\alpha_2\vec{\sigma}_1\cdot\vec{\sigma}_5-\frac{\alpha_2^2}{4b^2}(1-\gamma^2)\vec{\rho}\cdot\vec{\sigma}_1\vec{\rho}\cdot\vec{\sigma}_5\Bigg]g\left(\frac{\alpha_2}{b^2},\vec{\rho}\right)\Bigg\}, \tag{B14}$$

$$V_{25}^{ex}(\vec{\rho},\vec{\rho}')^{14}=\frac{4\pi\alpha_s C_{25}^t}{(\pi b^2/\alpha_1)^{3/2}}f_{25}^t(\vec{\rho},\vec{\rho}')_{ex}\Bigg\{g\left(\frac{\alpha_2}{b^2},\vec{\rho}+\vec{\rho}'\right)-\left(\frac{m_1^2+m_2^2}{8m_1^2m_2^2}+\frac{\vec{\sigma}_2\cdot\vec{\sigma}_5}{4m_1m_2}\right)-\frac{1}{4(m_1+m_2)^2b^2}\Bigg[\frac{6}{\alpha_1}-\frac{(\beta_2-\alpha_2)^2}{\alpha_1^2b^2}(\vec{\rho}-\vec{\rho}')^2$$
$$+\frac{\alpha_2(\alpha_1-\beta_1)}{2\alpha_1b^2}i(1-\gamma)(\vec{\rho}\times\vec{\rho}')\cdot\left[\left(1+\frac{m_2}{m_1}\right)\vec{\sigma}_2-\left(1+\frac{m_1}{m_2}\right)\vec{\sigma}_5\right]\Bigg]g\left(\frac{\alpha_2}{b^2},\vec{\rho}+\vec{\rho}'\right)g\left(\frac{\alpha_2}{b^2},\vec{\rho}+\vec{\rho}'\right)-\frac{1}{4m_1m_2b^2}$$
$$\times\Bigg[6\alpha_2+\frac{\alpha_2}{b^2}\left(\alpha_1-\frac{\beta_1}{\alpha_1}-2\alpha_2\beta_2\right)(\vec{\rho}-\vec{\rho}')^2-\alpha_2\vec{\sigma}_2\cdot\vec{\sigma}_5+\frac{\alpha_2^2}{2b^2}i(1+\gamma)(\vec{\rho}\times\vec{\rho}')\cdot\left[\left(2+\frac{m_2}{m_1}\right)\vec{\sigma}_2+\left(2+\frac{m_1}{m_2}\right)\vec{\sigma}_5\right]$$
$$-\frac{\alpha_2^2}{4b^2}(1-\gamma^2)(\vec{\rho}+\vec{\rho}')\cdot\vec{\sigma}_2(\vec{\rho}+\vec{\rho}')\cdot\vec{\sigma}_5\Bigg]g\left(\frac{\alpha_2}{b^2},\vec{\rho}+\vec{\rho}'\right)\Bigg\}, \tag{B15}$$

$$V_{35}^{ex}(\vec{\rho},\vec{\rho}')^{14}=\frac{4\pi\alpha_s C_{35}^t}{(\pi b^2/\alpha_1)^{3/2}}f_{25}^t(\vec{\rho},\vec{\rho}')_{ex}\Bigg\{g\left(\frac{\alpha_2}{b^2},\vec{\rho}+\vec{\rho}'\right)-\left(\frac{m_1^2+m_2^2}{8m_1^2m_2^2}+\frac{\vec{\sigma}_3\cdot\vec{\sigma}_5}{4m_1m_2}\right)-\frac{1}{4(m_1+m_2)^2b^2}\Bigg[\frac{6}{\alpha_1}-\frac{(\beta_2-\alpha_2)^2}{\alpha_1^2b^2}(\vec{\rho}-\vec{\rho}')^2$$
$$+\frac{\alpha_2(\alpha_1-\beta_1)}{2\alpha_1b^2}i(1-\gamma)(\vec{\rho}\times\vec{\rho}')\cdot\left[\left(1+\frac{m_2}{m_1}\right)\vec{\sigma}_3-\left(2+\frac{m_1}{m_2}\right)\vec{\sigma}_5\right]\Bigg]g\left(\frac{\alpha_2}{b^2},\vec{\rho}+\vec{\rho}'\right)-\frac{1}{4m_1m_2b^2}\Bigg[6\alpha_2+\frac{\alpha_2}{b^2}\Bigg(\alpha_1-\frac{\beta_1}{\alpha_1}$$
$$-2\alpha_2\beta_2\Bigg)(\vec{\rho}-\vec{\rho}')^2-\alpha_2\vec{\sigma}_3\cdot\vec{\sigma}_5+\frac{\alpha_2^2}{2b^2}i(1+\gamma)(\vec{\rho}\times\vec{\rho}')\cdot\left[\left(2+\frac{m_2}{m_1}\right)\vec{\sigma}_3+\left(2+\frac{m_1}{m_2}\right)\vec{\sigma}_5\right]$$
$$-\frac{\alpha_2^2}{4b^2}(1-\gamma^2)(\vec{\rho}+\vec{\rho}')\cdot\vec{\sigma}_3(\vec{\rho}+\vec{\rho}')\cdot\vec{\sigma}_5\Bigg]g\left(\frac{\alpha_2}{b^2},\vec{\rho}+\vec{\rho}'\right)\Bigg\}, \tag{B16}$$

$$V_{45}^{ex}(\vec{\rho},\vec{\rho}')^{14}=\frac{4\pi\alpha_s C_{45}^t}{(\pi b^2/\alpha_1)^{3/2}}f_{15}^t(\vec{\rho}',\vec{\rho})_{ex}\Bigg\{g\left(\frac{\alpha_2}{b^2},\vec{\rho}'\right)-\left(\frac{m_1^2+m_2^2}{8m_1^2m_2^2}+\frac{\vec{\sigma}_4\cdot\vec{\sigma}_5}{4m_1m_2}\right)-\frac{1}{4(m_1+m_2)^2b^2}\Bigg[\frac{6}{\alpha_1}-\frac{(\alpha_1\vec{\rho}'-\beta_1\vec{\rho}'+\beta_1\vec{\rho})^2}{\alpha_1^2b^2}$$
$$-\frac{\alpha_2\beta_1}{4\alpha_1b^2}i(1-\gamma)(\vec{\rho}'\times\vec{\rho})\cdot\left[\left(1+\frac{m_2}{m_1}\right)\vec{\sigma}_4-\left(1+\frac{m_1}{m_2}\right)\vec{\sigma}_5\right]\Bigg]g\left(\frac{\alpha_2}{b^2},\vec{\rho}'\right)-\frac{1}{4m_1m_2b^2}\Bigg[6\alpha_2-\frac{\alpha_2(\alpha_1-\alpha_2)\beta_1}{\alpha_1b^2}\vec{\rho}\cdot\vec{\rho}'$$
$$-\frac{\alpha_2(\alpha_1-\beta_1)^2-\alpha_2\beta_1\beta_2}{\alpha_1b^2}\vec{\rho}'^2-\alpha_2\vec{\sigma}_4\cdot\vec{\sigma}_5-\frac{\alpha_2^2}{4b^2}(1-\gamma^2)\vec{\rho}'\cdot\vec{\sigma}_4\vec{\rho}'\cdot\vec{\sigma}_5\Bigg]g\left(\frac{\alpha_2}{b^2},\vec{\rho}'\right)\Bigg\}, \tag{B17}$$

in which $\alpha_1=m_1/(m_1+m_2)$ and $\alpha_2=m_2/(m_1+m_2)$. The other exchanged potential $V_t^{ex}(\vec{\rho},\vec{\rho}')^{24}$ and $V_t^{ex}(\vec{\rho},\vec{\rho}')^{34}$ can directly be written out by changing the superscripts 14 to 24 and 34.

The terms of the direct part of the potential in Eq. (B3) are shown below,

$$V_{24}^D(\vec{\rho},\vec{\rho}')=\frac{4\pi\alpha_s C_{24}^t}{(2\pi b^2)^{3/2}}f_{24}^t(\vec{\rho},\vec{\rho}')_D\Bigg\{g\left(\frac{1}{2b^2},\vec{\rho}+\vec{\rho}'\right)+\frac{1}{4m_1^2}(1-\vec{\sigma}_2\cdot\vec{\sigma}_4)-\frac{1}{4m_1^2b^2}\Bigg[6-\frac{1}{2}\vec{\sigma}_2\cdot\vec{\sigma}_4-\frac{(\beta_2-\beta_1)^2}{4b^2}\vec{\rho}^2$$
$$+i\frac{3}{8b^2}(1+\gamma)(\vec{\rho}\times\vec{\rho}')\cdot(\vec{\sigma}_2+\vec{\sigma}_4)-\frac{1}{4b^2}(\vec{\rho}-\vec{\rho}')^2+i\frac{\beta_2-\beta_1}{8b^2}(1-\gamma)(\vec{\rho}\times\vec{\rho}')\cdot(\vec{\sigma}_2-\vec{\sigma}_4)+\frac{1}{16b^2}(1+\gamma^2)$$
$$\times(\vec{\rho}+\vec{\rho}')\cdot\vec{\sigma}_2(\vec{\rho}+\vec{\rho}')\cdot\vec{\sigma}_4\Bigg]g\left(\frac{1}{2b^2},\vec{\rho}+\vec{\rho}'\right)\Bigg\}, \tag{B18}$$

where

$$f_{24}^t(\vec{\rho},\vec{\rho}')_D=e^{-[(3\beta_2+1)/4b^2](\vec{\rho}-\vec{\rho}')^2-(3/16b^2)(\vec{\rho}+\vec{\rho}')^2}. \tag{B19}$$

The terms $V_{14}^D(\vec{\rho},\vec{\rho}')$ and $V_{34}^D(\vec{\rho},\vec{\rho}')$ in Eq. (B3) have the same form as shown above except for the subscripts 24 being changed to 14 and 34.

The term $V_{25}^D(\vec{\rho},\vec{\rho}')$ in Eq. (B3) is of the form

$$V_{25}^D(\vec{\rho},\vec{\rho}')=\frac{4\pi\alpha_s C_{25}^t}{(\pi b^2/\alpha_1)^{3/2}}f_{25}^t(\vec{\rho},\vec{\rho}')_D\Bigg\{g\left(\frac{\alpha_2}{b^2},\vec{\rho}+\vec{\rho}'\right)-\left(\frac{m_1^2+m_2^2}{8m_1^2m_2^2}+\frac{\vec{\sigma}_2\cdot\vec{\sigma}_5}{4m_1m_2}\right)-\frac{1}{4(m_1+m_2)^2b^2}\Bigg[\frac{6}{\alpha_1}-\frac{(\beta_2-\alpha_2)^2}{\alpha_1^2b^2}(\vec{\rho}-\vec{\rho}')^2$$
$$+\frac{\alpha_1-\beta_1}{2\alpha b^2}i(1+\gamma)(\vec{\rho}\times\vec{\rho}')\cdot\left[\left(1+\frac{m_2}{m_1}\right)\vec{\sigma}_2-\left(1+\frac{m_1}{m_2}\right)\vec{\sigma}_5\right]\Bigg]g\left(\frac{\alpha_2}{b^2},\vec{\rho}+\vec{\rho}'\right)-\frac{1}{4m_1m_2b^2}\Bigg[6\alpha_2+\frac{\alpha_2}{b^2}\Bigg(\alpha_1-\frac{\beta_1}{\alpha_1}$$
$$-2\alpha_2\beta_2\Bigg)(\vec{\rho}-\vec{\rho}')^2-\alpha_2\vec{\sigma}_2\cdot\vec{\sigma}_5+\frac{\alpha_2^2}{2b^2}i(1+\gamma)(\vec{\rho}\times\vec{\rho}')\cdot\left[\left(2+\frac{m_2}{m_1}\right)\vec{\sigma}_2+\left(2+\frac{m_1}{m_2}\right)\vec{\sigma}_5\right]$$
$$-\frac{\alpha_2^2}{4b^2}(1-\gamma^2)(\vec{\rho}+\vec{\rho}')\cdot\vec{\sigma}_2(\vec{\rho}+\vec{\rho}')\cdot\vec{\sigma}_5\Bigg]g\left(\frac{\alpha_2}{b^2},\vec{\rho}+\vec{\rho}'\right)\Bigg\}, \tag{B20}$$

where

$$f^t_{25}(\vec{\rho},\vec{\rho}')_D = e^{-[(3\beta_2-\beta_1^2)/4b^2](\vec{\rho}-\vec{\rho}')^2-(3\alpha_2/8b^2)(\vec{\rho}+\vec{\rho}')^2}. \tag{B21}$$

The remaining two terms in Eq. (B3) are of the same form as given above, except for the subscripts 25 being replaced by 15 and 35.

Let us turn to the $\bar{K}N$ interaction potential. For the $\bar{K}N$ interaction, there is only a direct part of the potential coming from the *t*-channel OGEP as represented in Eqs. (B3), (B18), and (B20) because there are no identical particles between the *N* cluster (*qqq*) and the $\bar{K}$ cluster ($\bar{q}s$). In addition, the nonlocal effective potential derived from the *s*-channel OGEP plays an essential role in the $\bar{K}N$ interaction. This potential can be written as

$$V^s(\vec{\rho},\vec{\rho}') = V^{s-d}_{14}(\vec{\rho},\vec{\rho}') + V^{s-d}_{24}(\vec{\rho},\vec{\rho}') + V^{s-d}_{34}(\vec{\rho},\vec{\rho}'), \tag{B22}$$

here $V^{s-d}_{14}(\vec{\rho},\vec{\rho}')$ denotes the direct term of the potential generated from the interaction of the quark 1 and the antiquark 4,

$$\begin{aligned} V^{s-d}_{14}(\vec{\rho},\vec{\rho}') = {} & \frac{4\pi\alpha_s F^a_{14}C^a_{14}}{(2\pi b^2)^{3/2}} f^s_{14}(\vec{\rho},\vec{\rho}')\Bigg\{(3+\vec{\sigma}_1\cdot\vec{\sigma}_4) \\ & - \frac{1}{4m_1^2b^2}\left[3-\frac{(\beta_2-\beta_1)^2}{4b^2}(\vec{\rho}-\vec{\rho}')^2\right] \\ & - \frac{1}{m_1^2b^2}(2+\vec{\sigma}_1\cdot\vec{\sigma}_4)\left(3-\frac{\vec{\rho}^2+\vec{\rho}'^2}{4b^2}\right) \\ & - i\frac{\beta_2-\beta_1}{8m_1^2b^2}(\vec{\rho}\times\vec{\rho}')\cdot(\vec{\sigma}_1-\vec{\sigma}_4) + \frac{\vec{\sigma}_1\cdot\vec{\sigma}_4}{m_1^2b^2} \\ & - \frac{1}{4m_1^2b^2}[\vec{\rho}\cdot\vec{\sigma}_1\vec{\rho}\cdot\vec{\sigma}_4 + \vec{\rho}'\cdot\vec{\sigma}_1\vec{\rho}'\cdot\vec{\sigma}_4]\Bigg\}, \end{aligned} \tag{B23}$$

where

$$f^s_{14}(\vec{\rho},\vec{\rho}')_D = e^{[(3\beta_2-1/2)/2b_1^2]\vec{\rho}\cdot\vec{\rho}'-[(3\beta_2+1/2)/4b_1^2](\vec{\rho}^2+\vec{\rho}'^2)}. \tag{B24}$$

The other two terms $V^{s-d}_{24}(\vec{\rho},\vec{\rho}')$ and $V^{s-d}_{34}(\vec{\rho},\vec{\rho}')$ can be written out from the above expression by the substitution of the subscripts 24 and 34 for 14.

The effective *KN* ($\bar{K}N$) potential derived from the interquark harmonic oscillator confining potential and quark interchanges are of simple expressions. They are represented as

$$\begin{aligned} V^{ex}_c(\vec{\rho},\vec{\rho}') = {} & -12b_1^2\omega^2\Bigg\{C_s^{24}\mu_{24}+C_s^{34}\mu_{34}+C_s^{12}\mu_{12}+C_s^{13}\mu_{13} \\ & + C_s^{14}\mu_{14} + \frac{1}{2\alpha_2}[C_s^{25}\mu_{25}+C_s^{35}\mu_{35}+C_s^{15}\mu_{15} \\ & + C_s^{45}\mu_{45}]\Bigg\}e^{-(\vec{\rho}\cdot\vec{\rho}'/2b^2)-(3\beta_2/4b^2)(\vec{\rho}-\vec{\rho}')^2}, \end{aligned} \tag{B25}$$

where the μ_{ij} denotes the reduced mass of interacting quarks *i* and *j* and the color factors are the same as the ones appearing in the *t*-channel potentials.

Apart from the potentials listed above, there are additional terms in the *KN* and $\bar{K}N$ potentials occurring in the resonating group equation, which arise from the kinetic term and the normalization term in the equation due to the effect of quark rearrangement. They are written as follows

$$\begin{aligned} T^{ex}(\vec{\rho},\vec{\rho}') = {} & (-3)\alpha^{3/2}\Bigg\{\frac{1}{2\mu}\left[\frac{\gamma_1}{2b^2}-\frac{(\gamma_1\vec{\rho}-\gamma_1\vec{\rho}'+\vec{\rho}')^2}{4b^4}\right] \\ & + \frac{1}{2\mu_1}\left[\frac{3}{4b^2}-\frac{\vec{\rho}'^2}{16b^4}\right] + \frac{1}{2\mu_2}\left[\frac{1}{4b^2}-\frac{\vec{\rho}'^2}{144b^4}\right] \\ & + \frac{1}{2\mu_3}\left[\frac{3\alpha_2}{2b^2}-\frac{\alpha_2^2\vec{\rho}'^2}{4b^4}\right]\Bigg\} f^{ex}_T(\vec{\rho},\vec{\rho}'), \end{aligned} \tag{B26}$$

where

$$f^{ex}_T(\vec{\rho},\vec{\rho}') = e^{-(\vec{\rho}\cdot\vec{\rho}'/2b^2)-(\gamma_1/4b^2)(\vec{\rho}-\vec{\rho}')^2}, \tag{B27}$$

$$\mu = \frac{3m_1(m_1+m_2)}{4m_1+m_2}, \quad \mu_1 = \frac{m_1}{2}, \quad \mu_2 = \frac{2m_1}{3}, \tag{B28}$$

$$\mu_3 = \frac{m_1m_2}{m_1+m_2}, \quad \gamma_1 = 3/(1/3+\alpha_1),$$

and

$$N^{ex}(\vec{\rho},\vec{\rho}') = -3E_re^{-(\vec{\rho}\cdot\vec{\rho}'/2b^2)-[(\beta_1^2+\beta_2^2)/2b^2](\vec{\rho}-\vec{\rho}')^2}, \tag{B29}$$

here E_r is the relative energy of two clusters.

The color-spin-isospin matrix elements of the above potentials are easily evaluated by using the CFS wave functions given in Appendix A.

APPENDIX C: DERIVATION OF PHASE SHIFT FORMULA

In this appendix, we briefly describe the derivation of the formula used to compute the phase shifts with a comment on the Born approximation. One of the authors of this paper, in his previous work on the relativistic Pauli-Schrödinger equation for two-body scattering states, which was proved to be equivalent to the corresponding Bethe-Salpeter equation [38], proved that in the relativistic case, the outgoing state wave function of the system under consideration may be written, in the position space, as

$$\psi(\vec{r}) = \varphi^0(\vec{r}) + f(\Omega_k)\frac{e^{ikr}}{r}, \tag{C1}$$

where $\varphi^0(\vec{r})$ is the wave function for free particles and $f(\Omega_k)$ the probability amplitude of the outgoing spherical wave. For a boson system, the wave function in Eq. (C1) is scalar, while, for a fermion system, the wave function is represented in the Pauli spinor space. In the unequal mass case, the amplitude $f(\Omega_k)$ is related to the transition amplitude T_{fi} in such a fashion,

$$f(\Omega_k) = -\frac{M(E)}{2\pi} T_{fi}, \tag{C2}$$

where

$$M(E) = \frac{E^4 - (m_K^2 - m_N^2)^2}{4E^3}, \tag{C3}$$

with E, m_K, and m_N being the total energy of the system, the kaon mass, and nucleon mass, and T_{fi} is the exact transition amplitude. The amplitude is defined by

$$T_{fi} = \langle \varphi_f^0 | V | \psi_i \rangle, \tag{C4}$$

where φ_f^0 is the plane wave function of final state, V stands for the interaction Hamiltonian operator, and ψ_i is the exact initial wave function which is determined by the following equation:

$$\psi_i = \varphi_i^0 + G^0 V \psi_i, \tag{C5}$$

in which φ_i^0 is the plane wave function of initial state and

$$G^0 = \frac{1}{E - H_0 + i\varepsilon}, \varepsilon \to 0^+, \tag{C6}$$

is the Green's function with H_0 being the free Hamiltonian. The solution of Eq. (C5) can formally be represented as

$$\psi_i = \frac{1}{1 - G^0 V} \varphi_i^0 = \sum_{n=0}^{\infty} [G^0 V]^n \varphi_i^0. \tag{C7}$$

In the lowest order Born approximation, $\psi_i = \varphi_i^0$ and, correspondingly, the transition amplitude in Eq. (C4) takes the form as given in Eq. (24).

Now we proceed to derive the formula written in Eq. (26). Let us expand the wave functions in Eq. (C1) in partial waves,

$$\psi_i = \sum_l \psi_l P_l(\cos\,\theta), \tag{C8}$$

$$f(\theta) = \sum_l f_l P_l(\cos\,\theta), \tag{C9}$$

and

$$\varphi_i^0 = e^{i\vec{k}\cdot\vec{r}} = \sum_l (2l+1) i^l j_l(kr) P_l(\cos\,\theta), \tag{C10}$$

where $P_l(\cos\,\theta)$ is the Legendre function of rank l. With these expansions, noticing the asymptotic behaviors of the spherical Bessel function $j_l(kr)$ and the function $\psi_l(r)$,

$$j_l(k) \overrightarrow{r \to \infty} \frac{1}{kr} \sin\left(kr - \frac{l\pi}{2}\right), \tag{C11}$$

$$\psi_l(r) \overrightarrow{r \to \infty} \frac{C_l}{r} \sin\left(kr - \frac{l\pi}{2} + \delta_l\right). \tag{C12}$$

One may find a result from Eq. (C1) such that

$$f_l = \frac{(2l+1)}{2ik}(e^{2i\delta_l} - 1). \tag{C13}$$

On the other hand, the transition amplitude may also be expanded in partial waves,

$$T_{fi} = 4\pi \sum_l (2l+1) T_l P_l(\cos\,\theta), \tag{C14}$$

where

$$T_l = \frac{1}{8\pi} \int_{-1}^{1} dx P_l(x) T_{fi}. \tag{C15}$$

Combining Eqs. (C2), (C9), (C13), and (C14), it is easy to derive the following relation:

$$e^{2i\delta_l} = 1 - 4iM(E)kT_l. \tag{C16}$$

When Eq. (C7) is substituted into Eq. (C4), we can write

$$T_{fi} = \sum_{n=0}^{\infty} T_{fi}^n, \tag{C17}$$

where

$$T_{fi}^n = \langle \varphi_f^0 | (VG^0)^n V | \phi_i^0 \rangle. \tag{C18}$$

On inserting Eq. (C17) into Eq. (C15), we have

$$T_l = \sum_{n=0}^{\infty} T_l^n, \tag{C19}$$

where

$$T_l^n = \frac{1}{8\pi} \int_{-1}^{1} dx P_l(x) T_{fi}^n. \tag{C20}$$

Upon substituting Eq. (C19) and the Taylor expansion of $e^{2i\delta_l}$ into Eq. (C16), one may find

$$\sum_{n=1}^{\infty} \frac{1}{n!} (2i\delta)^n = -i4M(E)k \sum_{n=0}^{\infty} T_l^n. \tag{C21}$$

From the above equality, it is clearly seen that there exists a one-to-one correspondence between the terms of the same order in the both series. When only the first term in each series is considered, we obtain

$$\delta_l = -2MkT_l(k), \tag{C22}$$

which is proportional to the interaction Hamiltonian V. This is just the formula for the phase shift which is given in the so-called Born approximation. If the phase shift is really proportional to the interaction Hamiltonian V as in the Born approximation, from the corresponding higher-order terms of the both series in Eq. (C21), we can write

$$(\delta_l)^{n+1} \approx -\frac{(n+1)!\, Mk}{2^{2-1} i^n} T_l^n, \tag{C23}$$

which is proportional to V^{n+1} and means that the nth terms in the both series in Eq. (C21) are approximately equal to each other as if Eq. (C23) is approximately given by tak-

ing the equality in Eq. (C22) to the $(n+1)$th power. If the relation in Eq. (C23) holds, we see that the formula in Eq. (C22) appears to be a good approximation.

APPENDIX D: NOTES ON QCD RENORMALIZATION

To help understanding of the renormalization formulas written in Sec. III, in this appendix, we give some explanations of the QCD renormalization. It is well-known that the *t*-channel OGEP in Eq. (4) and the *s*-channel OGEP in Eq. (6) are usually derived from the lowest-order *S*-matrix elements given by the tree Feynman diagrams representing, respectively, the quark-quark (or quark-antiquark) scattering and quark-antiquark annihilation processes in the nonrelativistic approximation of the order p^2/m^2. As an example, we write the lowest order *S*-matrix element for two-quark scattering as follows:

$$S_{fi}^{(0)} = \bar{u}^{(0)}(p_1) ig\gamma^\mu T^a u^{(0)}(q_1) iD_{\mu\nu}^{(0)ab}(k) \bar{u}^{(0)}(p_2) ig\gamma^\nu T^b u^{(0)}(q_2), \tag{D1}$$

where $u^{(0)}(p)$ is the free quark wave function, $\bar{u}^{(0)}(p_1)$ is its Dirac conjugate (here the spin indices of the spinor functions are suppressed for simplicity), $iD_{\mu\nu}^{(0)ab}(k)$ is the gluon free propagator with $k=p_1-q_1=q_2-p_2$, and $ig\gamma^\mu T^a$ is the bare vertex with g being the coupling constant and T^a the color matrix. Correspondingly, the exact *S*-matrix element given by the one-gluon exchange interaction is represented as

$$S_{fi} = \bar{u}(p_1)\Gamma^{a\mu}(p_1, q_1) u(q_1) iD_{\mu\nu}^{ab}(k) \bar{u}(p_2)\Gamma^{a\nu}(p_2, q_2) u(q_2), \tag{D2}$$

where $u(p)$, $iD_{\mu\nu}^{ab}(k)$, and $\Gamma^{a\mu}(p,q)$ denote the full (or say, dressed) quark wave function, gluon propagator, and quark-gluon vertex, respectively, in which all higher order perturbative corrections are included. According to the well-known renormalization relations,

$$u(p) = \sqrt{Z_2} u_R(p), \bar{u}(p) = \sqrt{Z_2}\bar{u}_R(p),$$

$$D_{\mu\nu}^{ab}(k) = Z_3 D_{R\mu\nu}^{ab}(k), \Gamma^{a\mu}(p,q) = Z_\Gamma \Gamma_R^{a\mu}(p,q), \tag{D3}$$

where the subscript R marks the renormalized quantities, and $\sqrt{Z_2}$, Z_3, and $Z_\Gamma = Z_2^{-1} Z_3^{-\frac{1}{2}}$ are the renormalization constants for the quark wave function, the gluon propagator, and the quark-gluon vertex, respectively, one can get from Eq. (D2) that

$$S_{fi} = \bar{u}_R(p_1)\Gamma_R^{a\mu}(p_1, q_1) u_R(q_1) iD_{R\mu\nu}^{ab}(k) \times \bar{u}_R(p_2)\Gamma_R^{a\nu}(p_2, q_2) u_R(q_2). \tag{D4}$$

As shown in Ref. [27], the renormalized quantities in the above can be determined by their renormalization group equations and their renormalization boundary conditions. The results given by solving the renormalization group equations are

$$u_R(p) = \exp\left[\frac{1}{2}\int_1^\lambda \frac{d\lambda}{\lambda}\gamma_2(\lambda)\right] u_R^{(0)}(p),$$

$$\bar{u}_R(p) = \exp\left[\frac{1}{2}\int_1^\lambda \frac{d\lambda}{\lambda}\gamma_2(\lambda)\right] \bar{u}_R^{(0)}(p),$$

$$D_{R\mu\nu}^{ab}(k) = \exp\left[\int \frac{d\lambda}{\lambda}\gamma_3(\lambda)\right] iD_{R\mu\nu}^{(0)ab}(k),$$

$$\Gamma_R^{a\mu}(p,q) = \exp\left[\int \frac{d\lambda}{\lambda}\gamma_\Gamma(\lambda)\right] ig_R(\lambda)\gamma^\mu T^a, \tag{D5}$$

where $u_R^{(0)}(p)$ and $\bar{u}_R^{(0)}(p)$ are of the same forms as the free wave functions except that the quark mass in them becomes the effective (running) one, $iD_{R\mu\nu}^{(0)ab}(k)$ formally is the same as the free propagator but the gauge parameter in it is replaced by the effective one, $g_R(\lambda)$ in the bare vertex $ig_R(\lambda)\gamma^\mu T^a$ is the effective coupling constant, and $\frac{1}{2}\gamma_2(\lambda)$, $\gamma_3(\lambda)$, and $\gamma_\Gamma(\lambda)$ are the anomalous dimensions defined by

$$\frac{1}{2}\gamma_2(\lambda) = \lambda\frac{d}{d\lambda}\ln\sqrt{Z_2(\lambda)},\ \gamma_3(\lambda) = \lambda\frac{d}{d\lambda}\ln Z_3(\lambda),$$

$$\gamma_\Gamma(\lambda) = \lambda\frac{d}{d\lambda}\ln Z_\Gamma(\lambda) = -\gamma_2(\lambda) - \frac{1}{2}\gamma_3(\lambda). \tag{D6}$$

On inserting Eq. (D5) into Eq. (D4), we see that the anomalous dimensions are all canceled out with each other. As a result, we have

$$S_{fi} = \bar{u}_R^{(0)}(p_1) ig_R(\lambda)\gamma^\mu T^a u_R^{(0)}(q_1) iD_{R\mu\nu}^{(0)ab}(k) \bar{u}_R^{(0)} \times (p_2) ig_R(\lambda)\gamma^\nu T^b u_R^{(0)}(q_2). \tag{D7}$$

This *S*-matrix element is completely the same as the one shown in Eq. (D1) except that the quark mass, the gauge parameter, and the coupling constant are replaced by the running ones. In the nonrelativistic approximation of order p^2/m^2, one may derive a OGEP from Eq. (D7), which in the Feynman gauge is just as that written in Eq. (4) with the coupling constant and quark mass being the effective ones. These effective quantities precisely represent the renormalization effect and at one-loop level, they are of the forms as given in Sec. III. For the *s*-channel OGEP, the discussion is completely the same.

Next, we would like to address the renormalization point. In the ordinary QCD renormalization performed in the minimal subtraction scheme, which is suitable in the large momentum limit because only in this limit the quark mass can be set to be zero, the renormalization point is chosen to be spacelike. This choice is suitable to the scattering process because in this case the transfer momentum, i.e., the variable of the gluon propagator in Eq. (D2) is spacelike. This can be seen from the following derivation:

$$k^2 = (p_1 - q_1)^2 = 2m^2 - 2\sqrt{\vec{p}_1^{\,2} + m^2}\sqrt{\vec{q}_1^{\,2} + m^2} + 2|\vec{p}_1||\vec{q}_1|\cos\theta, \tag{D8}$$

in the high energy limit, we can set $m \approx 0$, therefore

$$k^2 \approx -2|\vec{p}_1||\vec{q}_1|(1-\cos\theta) \leqslant 0. \tag{D9}$$

In the low-energy domain, since

$$\sqrt{\vec{p}^2 + m^2} \approx m + \frac{\vec{p}^2}{2m^2}, \tag{D10}$$

Eq. (D8) can be approximated as

$$k^2 \approx -(\vec{p}_1 - \vec{q}_1)^2 \leqslant 0. \tag{D11}$$

So, for the *t*-channel OGEP, it is suitable to use the effective coupling constant and quark mass given by the subtraction performed at spacelike renormalization point; while, for the annihilation process, the momentum in the gluon propagator is timelike because in this case $k=p_1+p_2=q_1+q_2$,

$$k^2 = (p_1 + p_2)^2 = 2m^2 + 2\sqrt{\vec{p}_1^{\,2} + m^2}\sqrt{\vec{p}_2^{\,2} + m^2} - 2|\vec{p}_1||\vec{p}_2|\cos\theta. \tag{D12}$$

In the large momentum limit, we can write

$$k^2 \approx 2|\vec{p}_1||\vec{p}_2|(1 - \cos\theta) \geqslant 0, \tag{D13}$$

in the low-energy regime, we have

$$k^2 \approx (\vec{p}_1 - \vec{p}_2)^2 \geqslant 0. \tag{D14}$$

Therefore, for the *s*-channel OGEP, it is appropriate to use the effective quantities given by the subtraction carried out at timelike renormalization point.

[1] A. De Rújula, H. Georgi, and S. L. Glashow, Phys. Rev. D **12**, 147 (1975).
[2] N. Isgur and G. Karl, Phys. Rev. D **18**, 4187 (1978); **19**, 2653 (1979).
[3] W. Lucha, F. F. Schoberl, and D. Gromes, Phys. Rep. **200**, 127 (1991), and references therein.
[4] J. J. Griffin and J. A. Wheeler, Phys. Rev. **108**, 311 (1957).
[5] M. Harvey, Nucl. Phys. **A352**, 326 (1981).
[6] M. Oka and K. Yazaki, Prog. Theor. Phys. **66**, 556 (1981).
[7] A. Faessler, E. Fernandez, G. Lubeck, and K. Shimizu, Nucl. Phys. **A402**, 555 (1983).
[8] I. Bender and H. G. Dosch, Z. Phys. C **13**, 69 (1982).
[9] H. J. Pirner and B. Povh, Phys. Lett. **114B**, 308 (1982).
[10] I. Bender, H. G. Dosch, H. J. Priner, and H. G. Kruse, Nucl. Phys. **A414**, 359 (1984).
[11] D. Mukhopadhyay and H. J. Pirner, Nucl. Phys. **A442**, 605 (1985).
[12] J. Weinstein and N. Isgur, Phys. Rev. D **27**, 588 (1983); **41**, 2236 (1990); **43**, 95 (1991).
[13] R. Müller, T. Schmeidl, and H. M. Hofmann, Z. Phys. A **334**, 451 (1989).
[14] T. Barnes, E. S. Swanson, and J. Weinstein, Phys. Rev. D **46**, 4868 (1992).
[15] T. Barnes and E. S. Swanson, Phys. Rev. D **46**, 131 (1992); Phys. Rev. C **49**, 1166 (1994).
[16] T. Barnes, N. Black, and E. S. Swanson, Phys. Rev. C **63**, 025204 (2001).
[17] N. Black, J. Phys. G **28**, 1953 (2002).
[18] S. Lemaire, J. Labarsouque, and B. Slivestre-Brac, Nucl. Phys. **A696**, 497 (2001).
[19] G. Q. Zhao, X. G. Jing, and J. C. Su, Phys. Rev. D **58**, 117503 (1998).
[20] J. X. Chen, Y. H. Cao, and J. C. Su, Phys. Rev. C **64**, 065201 (2001).
[21] J. C. Su, Y. B. Dong, and S. S. Wu, J. Phys. G **18**, 1347 (1992).
[22] J. C. Su and S. S. Wu, Chin. Phys. **8**, 978 (1989); J. C. Su, Z. Q. Chen, and S. S. Wu, Nucl. Phys. **A254**, 615 (1991).
[23] J. C. Su, L. Y. Shan, and Y. H. Cao, Commun. Theor. Phys. **36**, 665 (2001).
[24] E. Braaten and Y. Q. Chen, Phys. Rev. Lett. **76**, 730 (1996).
[25] Feng Yuan, Cong-Feng Qiao, and Kuang-Ta Chao, Phys. Rev. D **56**, 321 (1997).
[26] Y. B. Dong, J. C. Su, and S. S. Wu, J. Phys. G **18**, 75 (1992).
[27] J. C. Su, X. X. Yi, and Y. H. Cao, J. Phys. G **25**, 2325 (1999).
[28] G. t'Hooft, Nucl. Phys. **B61**, 455 (1973); W. A. Bardeen, A. J. Buras, D. W. Duke, and T. Muta, Phys. Rev. D **18**, 3998 (1978).
[29] J. S. Hyslop, R. A. Arndt, L. D. Roper, and R. L. Workman, Phys. Rev. D **46**, 961 (1992).
[30] K. Hashimoto, Phys. Rev. C **29**, 1377 (1984).
[31] J. D. Davies, G. J. Pyle, G. T. A. Squier, C. J. Batty, S. F. Biagi, S. D. Hoath, P. Sharman and A. S. Clough, Phys. Lett. **83B**, 55 (1979).
[32] M. Izycki, G. Backenstoss, L. Tauscher, P. Blum, R. Guigas, N. Hassler, H. Koch, H. Poth, K. Fransson, A. Nilsson, P. Pavlopoulos, and K. Zioutas, Z. Phys. A **297**, 11 (1980).
[33] P. M. Bird, A. S. Clough, and K. R. Parker, Nucl. Phys. **A404**, 482 (1983).
[34] M. Iwasaki *et al.*, Phys. Rev. Lett. **78**, 3067 (1997).
[35] A. D. Martin, Nucl. Phys. **B179**, 33 (1981).
[36] B. R. Martin and M. Sakit, Phys. Rev. **183**, 1352 (1969).
[37] T. Waas, N. Kaiser, and W. Weise, Phys. Lett. B **365**, 12 (1996).
[38] J. C. Su, Commun. Theor. Phys. **18**, 327 (1992).
[39] M. Lutz and E. Kolomeitsev, nucl-th/0004021.